Comparison of myoplasmic calcium movements during excitation-contraction coupling in frog twitch and mouse fast-twitch muscle fibers

Stephen Hollingworth and Stephen M. Baylor

Department of Physiology, Perelman School of Medicine at the University of Pennsylvania, Philadelphia, PA 19104

Single twitch fibers from frog leg muscles were isolated by dissection and micro-injected with furaptra, a rapidly responding fluorescent Ca²⁺ indicator. Indicator resting fluorescence (F_R) and the change evoked by an action potential (ΔF) were measured at long sarcomere length (16°C); $\Delta F/F_R$ was scaled to units of Δf_{CaD} , the change in fraction of the indicator in the Ca^{2+} -bound form. Δf_{CaD} was simulated with a multicompartment model of the underlying myoplasmic Ca²⁺ movements, and the results were compared with previous measurements and analyses in mouse fast-twitch fibers. In frog fibers, sarcoplasmic reticulum (SR) Ca²⁺ release evoked by an action potential appears to be the sum of two components. The time course of the first component is similar to that of the entire Ca²⁺ release waveform in mouse fibers, whereas that of the second component is severalfold slower; the fractional release amounts are ~ 0.8 (first component) and ~ 0.2 (second component). Similar results were obtained in frog simulations with a modified model that permitted competition between Mg²⁺ and Ca²⁺ for occupancy of the regulatory sites on troponin. An anatomical basis for two release components in frog fibers is the presence of both junctional and parajunctional SR Ca²⁺ release channels (ryanodine receptors [RyRs]), whereas mouse fibers (usually) have only junctional RyRs. Also, frog fibers have two RyR isoforms, RyRα and RyRβ, whereas the mouse fibers (usually) have only one, RyR1. Our simulations suggest that the second release component in frog fibers functions to supply extra Ca²⁺ to activate troponin, which, in mouse fibers, is not needed because of the more favorable location of their triadic junctions (near the middle of the thin filament). We speculate that, in general, parajunctional RyRs permit increased myofilament activation in fibers whose triadic junctions are located at the z-line.

INTRODUCTION

The Journal of General Physiology

In vertebrate skeletal muscle fibers, action potentials (APs) control contractile activity by eliciting rapid changes in the myoplasmic free Ca²+ concentration (Δ [Ca²+]). The amplitude and time course of the spatially averaged Δ [Ca²+] signal can be estimated with an appropriately chosen low-affinity Ca²+ indicator microinjected into the myoplasm (for review see Baylor and Hollingworth, 2011). From the indicator signal, kinetic modeling can be used to estimate the underlying Ca²+ movements, including (a) the release of Ca²+ from the SR, (b) the binding of Ca²+ to the major myoplasmic Ca²+ buffers (troponin, ATP, parvalbumin, and the SR Ca²+ pump), and (c) the reuptake of Ca²+ into the SR by the SR Ca²+ pumps.

The first detailed estimates of myoplasmic Ca^{2+} movements in skeletal muscle were carried out with single-compartment (spatially averaged) kinetic models (e.g., Robertson et al., 1981; Baylor et al., 1983; Melzer et al., 1987; Baylor and Hollingworth, 1988). A deficiency in single-compartment modeling is that it does not account for the substantial spatial gradients in $\Delta[Ca^{2+}]$ that arise within the sarcomere because of the restricted locations of the SR Ca^{2+} release sites (Cannell and Allen, 1984;

Escobar et al., 1994; Hollingworth et al., 2000; Gómez et al., 2006). More accurate estimates of the myoplasmic Ca²⁺ movements can be obtained with multicompartment (spatially resolved) modeling, in which Ca²⁺ release, Ca²⁺ pumping, and Ca²⁺ binding to the myoplasmic Ca²⁺ buffers are calculated for different locations within the sarcomere.

The first such multicompartment model analyzed Ca²⁺ transients measured in frog twitch fibers with aequorin during twitches and brief tetani (Cannell and Allen, 1984). Subsequently, multicompartment modeling was used to analyze frog Ca²⁺ transients measured with furaptra (Baylor and Hollingworth, 1998). Furaptra is a low-affinity rapidly responding Ca²⁺ indicator with some sensitivity to Mg²⁺ (Raju et al., 1989); the indicator's myoplasmic fluorescence signal is thought to provide an accurate estimate of Δ [Ca²⁺] elicited by APs (Konishi et al., 1991; Baylor and Hollingworth, 2011). Thus, multicompartment modeling based on the furaptra Ca²⁺ signal likely gives reasonably accurate estimates of the amplitude and time course of SR Ca²⁺ release and the associated myoplasmic Ca²⁺ movements.

Correspondence to Stephen M. Baylor: baylor@mail.med.upenn.edu Abbreviations used in this paper: AP, action potential; CICR, Ca²+induced Ca²+ release; DHPR, dihydropyridine receptor; E-C, excitation-contraction; EDL, extensor digitorum longus; FDHM, full duration at half maximum; RyR, ryanodine receptor; VICR, voltage-induced Ca²+ release.

^{© 2013} Hollingworth and Baylor This article is distributed under the terms of an Attribution–Noncommercial–Share Alike–No Mirror Sites license for the first six months after the publication date (see http://www.rupress.org/terms). After six months it is available under a Creative Commons License (Attribution–Noncommercial–Share Alike 3.0 Unported license, as described at http://creativecommons.org/licenses/bv-nc-sa/3.0/).

The aim of this study was to compare measurements and multicompartment simulations of the furaptra Ca²⁺ signal in frog twitch fibers with those recently carried out in mouse fast-twitch fibers of extensor digitorum longus (EDL) muscle (Baylor and Hollingworth, 2007, 2012). Comparisons of this type based on the use of identical techniques are of interest because of the finding that the SR Ca²⁺ release channels (also known as ryanodine receptors [RyRs]) differ in two important respects in adult skeletal fibers of amphibians and mammals. First, in mammals, a single RyR isoform, RyR1, is usually found, although there are small amounts of a second isoform, RyR3, in some fibers of specialized muscles such as diaphragm (e.g., Sorrentino, 2003). In contrast, in amphibians, two isoforms, denoted RyRα and RyRβ, are found in approximately equal numbers in all major skeletal muscles (Olivares et al., 1991; Lai et al., 1992; Murayama and Ogawa, 1992). The amino acid composition of RyRα and RyRB is analogous, respectively, to that of the mammalian RyR1 and RyR3 isoforms (Oyamada et al., 1994; Ottini et al., 1996).

A second difference between mammalian and amphibian RyRs concerns their anatomical arrangement at the triadic junctions, which are the sites of SR Ca²⁺ release during excitation-contraction (E-C) coupling. In mammals, the triadic junctions are located near the middle of the thin filament (Smith, 1966; Eisenberg, 1983; Brown et al., 1998), whereas, in amphibians, they are located near the z-line (e.g., Franzini-Armstrong, 1975). In addition, mammalian RyRs are found in a standard "junctional" configuration (Franzini-Armstrong and Nunzi, 1983; Block et al., 1988), which consists of a doublerowed array of RyRs in the region of the SR membrane located directly opposite a junctional region of transverse tubular (T-tubular) membrane (Fig. 1). The latter region contains its own double-rowed array of particles, the dihydropyridine receptors (DHPRs), which are the voltage sensors of E-C coupling (Ríos and Brum, 1987; Tanabe et al., 1988). The DHPRs are organized into groups of four, called "tetrads" (Franzini-Armstrong, 1984; Block et al., 1988; also see Fig. 1). The tetrads and junctional RyRs are present in a 1:2 stoichiometry, with one of every two RyRs positioned opposite a tetrad and the other positioned opposite a vacant space in the tetradic array (Franzini-Armstrong and Kish, 1995; Paolini et al., 2004). In amphibians, in contrast, only about half of all RyRs reside in this junctional configuration; the other half reside in a configuration termed "parajunctional" (Felder and Franzini-Armstrong, 2002). Parajunctional RyRs are found in double-rowed arrays that are offset \sim 40 nm on either side of a junctional row (Fig. 1). The parajunctional arrays are incomplete, being, on average, only half-filled with RyRs, whereas the junctional arrays are fully filled. It is hypothesized that the junctional arrays contain only the RyRα isoform and the parajunctional arrays only the RyRB isoform (Felder and

Franzini-Armstrong, 2002). Overall, this arrangement would be consistent with the \sim 50:50 numerical ratio of RyR α to RyR β molecules reported in amphibians.

We report here that, in intact frog twitch fibers microinjected with furaptra and stimulated by an AP, the SR Ca²⁺ release waveform estimated with multicompartment modeling can be described as the sum of two kinetic components. The first component, with a fractional release amount of \sim 0.8, has a time course that is similar to that of the entire SR Ca²⁺ release waveform estimated previously in fast-twitch and slow-twitch mouse fibers at the same temperature (16°C). The full duration at half maximum (FDHM) of these three release waveforms is \sim 2 ms (frog twitch), \sim 1.6 ms (mouse fast twitch; Baylor and Hollingworth, 2007), and ~ 1.7 ms (mouse slow twitch; Hollingworth et al., 2012). Based on this similarity, it is reasonable to believe that the first release component in frog fibers and the entire release waveform in both types of mouse fibers are caused by a similar mechanism, namely, activation of junctional RyRs. The second release component in frog fibers, with a fractional release amount of \sim 0.2, is substantially slower, with an estimated FDHM of \sim 9 ms. We speculate that this release component is caused by Ca²⁺ release through parajunctional RyRs, the activation of which is secondary to that of junctional RyRs.

Our furaptra measurements in frog fibers were also analyzed under the hypothesis that Mg²⁺ competes with Ca²⁺ for occupation of the regulatory sites on troponin.

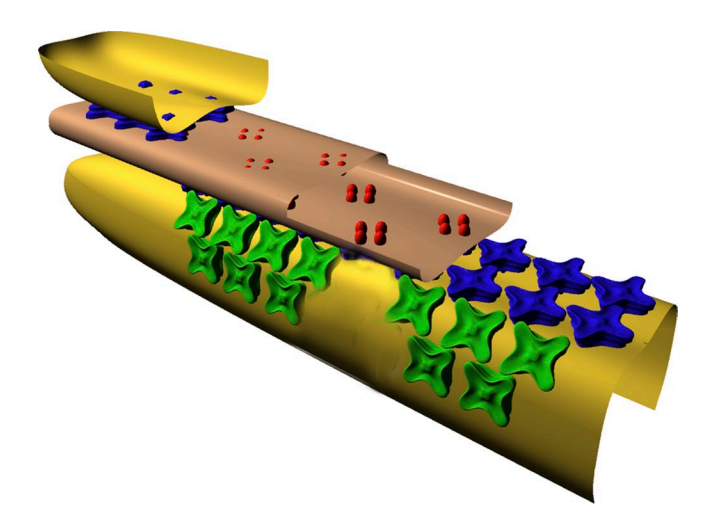


Figure 1. Cut-away schematic (Felder and Franzini-Armstrong, 2002) of essential E-C coupling molecules and membranes at the triadic junction of vertebrate skeletal muscle fibers. The diagram shows a junctional T-tubular membrane (light brown) flanked by two terminal-cisternal membranes of the sarcoplasmic reticulum (yellow). DHPR molecules (red) reside in the T-membrane; junctional RyRs (blue) and parajunctional RyRs (green) reside in the SR membrane. The parajunctional RyRs do not appear to contact the junctional RyRs (Felder and Franzini-Armstrong, 2002). See Introduction for further information, including the types of fibers in which parajunctional receptors are found. Copyright (2002) National Academy of Sciences, USA.

This possibility is supported by several studies in the literature (e.g., Godt and Lindley, 1982; Morimoto, 1991; Allen et al., 1992; Davis et al., 2002), but, to our knowledge, has not yet been considered in analyses of $\Delta [\text{Ca}^{2+}]$ measurements in intact muscle cells. Estimates of SR Ca^{2+} release with our multicompartment modeling are not strongly affected by the assumption that Mg^{2+} binds to the troponin regulatory sites with a moderate affinity (Mg^{2+} -troponin dissociation constant = 2 mM; myoplasmic free [Mg^{2+}] = 1 mM). The main effects of including competition between Ca^{2+} and Mg^{2+} for the regulatory sites are (a) to slightly reduce the estimated amount of SR Ca^{2+} release elicited by an AP, with little effect on the time course of release; and (b) to modestly reduce and delay the occupancy of the regulatory sites with Ca^{2+} .

MATERIALS AND METHODS

Ethical approval

Animal protocols were approved by the Institutional Animal Care and Use Committee of the University of Pennsylvania.

Experimental measurements

The experiments were carried out as described previously (Konishi et al., 1991; Zhao et al., 1996). An intact single fiber from a frog leg muscle (semitendinosus or iliofibularis) was isolated by dissection, mounted on an optical bench apparatus, and bathed in a Ringer's solution (16°C) that contained (in mM): 120 NaCl, 2.5 KCl, 1.8 CaCl₂, and 5 PIPES, pH, 7.1. To minimize movement artifacts in the optical recordings, the fiber was stretched to a long sarcomere length $(3.7 \pm 0.1 \, \mu \text{m}; \text{mean} \pm \text{SEM}, n = 7); \text{ in some experiments, } 5 \, \mu \text{M}$ N-benzyl-p-toluene sulphonamide (BTS) was included in Ringer's solution to further reduce fiber movement. As shown previously (Cheung et al., 2002), BTS at this concentration is effective at suppressing the fiber's contractile response without affecting the furaptra Ca²⁺ transient nor, by implication, the underlying myoplasmic Ca²⁺ movements. The fiber was pressure injected with the potassiumsalt form of furaptra (Raju et al., 1989). The indicator fluorescence at rest (F_R) and changes elicited by an AP (ΔF) were measured from a 300-um length of fiber that contained \sim 0.1 mM furaptra.

Although, in general, the diameter of frog twitch fibers is larger than that of mouse fast-twitch fibers from EDL muscle (the mouse fibers referenced in Results), an effort was made to match the diameters of the frog fibers to those of the mouse fibers. The diameter of each injected fiber was measured in one transverse dimension with a calibrated graticule. For the seven frog fibers of this study, the mean diameter was $53 \pm 4 \, \mu m$; the mean diameter for the eight mouse EDL fibers was $41 \pm 2 \, \mu m$.

 $\Delta F/F_R$ was converted to Δf_{CaD} , the change in the fraction of furaptra in the Ca²⁺-bound form, with Eq. 1 (which is appropriate for excitation and emission wavelengths of 390–430 nm and 470–590 nm, respectively; Baylor and Hollingworth, 2003):

$$\Delta f_{CaD} = -1.07 \times (\Delta F/F_R). \tag{1}$$

From $\Delta f_{\text{CaD}},$ a first estimate of spatially averaged $\Delta \text{[Ca}^{2+}\text{]}$ was obtained with Eq. 2:

$$\Delta[\mathrm{Ca}^{2+}] = \mathrm{K}_{\mathrm{D.Ca}} \times \Delta f_{\mathrm{CaD}} / (1 - \Delta f_{\mathrm{CaD}}). \tag{2}$$

 $K_{D,Ca}$, the apparent dissociation constant of furaptra for Ca^{2+} in the myoplasm, was assumed to be 96 μM . Because large gradients

in $[Ca^{2+}]$ exist in myoplasm during activity, $\Delta[Ca^{2+}]$ estimated with Eq. 2 likely involves some error (Hirota et al., 1989; Baylor and Hollingworth, 1998, 2007). A more accurate estimate of $\Delta[Ca^{2+}]$ is thought to be obtained with multicompartment modeling (next section and Results).

Model simulations

Myoplasmic Ca²⁺ movements elicited by APs were simulated with an 18-compartment reaction-diffusion model of a half-sarcomere of a myofibril (Fig. 2). The calculations were carried out with MLAB (Civilized Software, Inc.). Most simulations were carried out with the same parameter values used previously for mouse fast-twitch fibers (Tables I–III of Baylor and Hollingworth, 2007). The mouse model represents an evolution of our first multicompartment model (used for frog fibers; Baylor and Hollingworth, 1998). The new features in the mouse model include a four-state scheme for the reaction between Ca²⁺ and furaptra, a three-state scheme for the reaction between Ca²⁺ and troponin, and a multistate scheme for the reaction between Ca²⁺ and the SR Ca²⁺ pump (Fig. 2 of Baylor and Hollingworth, 2007). Table 1 lists the concentrations of the myoplasmic Ca²⁺ buffers in the model and the diffusion coefficients of the mobile constituents.

A significant difference between the frog and mouse models is the site of SR Ca²⁺ release (large downward arrows in Fig. 2). In the frog model, Ca²⁺ enters the myoplasm in the compartment at the outer surface of the myofibril next to the z-line, which approximates the location of the SR release sites in amphibian fibers (Franzini-Armstrong, 1975; Escobar et al., 1994; Tsugorka et al., 1995; Klein et al., 1996; Hollingworth et al., 2000). In the mouse model, the release compartment is offset to the middle of the troponincontaining region (middle of the thin filament), which approximates

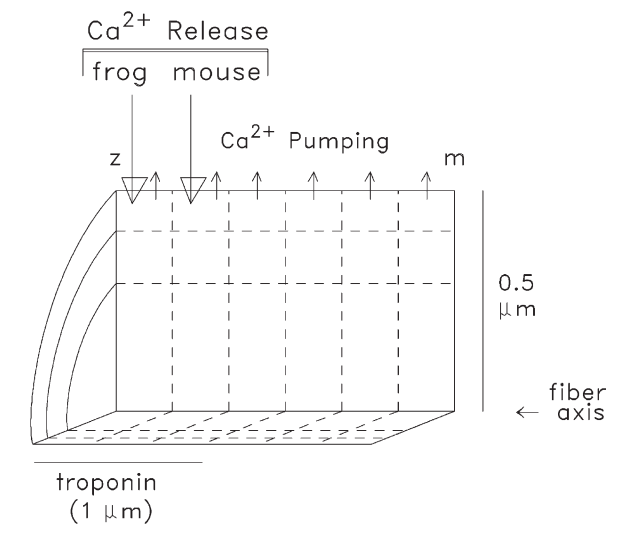


Figure 2. Geometry of the multicompartment model used in the simulations. The myoplasm of a half-sarcomere of one myofibril is divided into 18 equal-volume compartments (6 longitudinal by 3 radial); "z" and "m" denote the locations of the z-line and m-line. SR Ca^{2+} release enters the compartment indicated by the large downward arrows, which differs according to fiber type. Ca^{2+} pumping takes place in the six outermost compartments (small upward arrows). Troponin is restricted to the nine compartments located within 1 µm of the z-line, the approximate length of the thin filament. The remaining constituents of the model (ATP, parvalbumin, and furaptra) have access to all compartments by diffusion. In the mouse simulations, the radius of the sarcomere (0.375 µm) is slightly smaller than depicted, a difference that, by itself, results in only very small differences in the calculations.

TABLE 1

Concentrations and diffusion coefficients assumed in the model for frog twitch fibers and mouse fast-twitch fibers (16°C)

Constituent	Concentration	Concentration of binding-sites	Diffusion coefficient
	μM	μM	$10^{-6} cm^2/s$
Free [Ca ²⁺]	0.050 (resting)	_	3
Free [Mg ²⁺]	1,000	_	_
Troponin	120	240 (Ca ²⁺ regulatory sites)	0
SR Ca ²⁺ pump	120	240 (Ca ²⁺ regulatory sites)	0
Parvalbumin	750	1,500 (Ca ²⁺ /Mg ²⁺ sites)	0.15
ATP	8,000	8,000 (Ca ²⁺ /Mg ²⁺ sites)	1.4
Furaptra	100	$100 (Ca^{2+}/Mg^{2+} sites)$	1.59
Protein	500	500 (furaptra sites)	0

All concentrations are spatially averaged and referred to the myoplasmic water volume; except for $[Ca^{2^+}]$ and $[Mg^{2^+}]$, total concentrations are given. Because these concentrations are spatially averaged and because troponin and the SR Ca^{2^+} pump molecules do not diffuse, the actual concentrations of troponin and the Ca^{2^+} pump in the relevant compartments of the multicompartment (Fig. 2) are 2.0 and 3.0, respectively, times the values listed here. The concentration of protein applies to the four-state furaptra reaction scheme (see Fig. 1 E and Table 2 E of Baylor and Hollingworth, 2007). Free $[Mg^{2^+}]$ is assumed to be constant during activity; pH (which affects the Ca^{2^+} pump reaction) is assumed to be 7 and constant. The diffusion coefficients of ATP and furaptra apply to both the Ca^{2^+} -free and Ca^{2^+} -bound forms; the diffusion coefficient for parvalbumin applies to the Ca^{2^+} -bound, Ca^{2^+} -bound, and metal-free forms. From Baylor and Hollingworth (2007).

the location of the release sites in mammalian fibers (Smith, 1966; Eisenberg, 1983; Brown et al., 1998; Gómez et al., 2006).

Activity in the model begins when an SR Ca^{2+} release flux enters the release compartment. This causes free $[Ca^{2+}]$ in that compartment to rise, thus driving (a) complexation of Ca^{2+} with its buffers and (b) the diffusion of Ca^{2+} and the mobile Ca^{2+} buffers across the compartment's boundaries. Analogous changes occur subsequently in the other compartments. The model thus yields compartment estimates of: (a) $\Delta[Ca^{2+}]$, (b) the changes in the concentration of Ca^{2+} bound to the myoplasmic Ca^{2+} buffers (troponin, $\Delta[CaTrop]$; ATP, $\Delta[CaATP]$; parvalbumin, $\Delta[CaParv]$; the SR Ca^{2+} pump, $\Delta[CaPump]$; and furaptra, $\Delta[CaDye]$), (c) the myoplasmic diffusion of free Ca^{2+} and of Ca^{2+} bound to the mobile Ca^{2+} buffers (ATP, parvalbumin, and furaptra), and (d) the reuptake of Ca^{2+} into the SR by the SR Ca^{2+} pumps ($\Delta[CaPumped]$). Examples of such changes in the individual compartments of the model have been given previously (mouse model; Baylor and Hollingworth, 2007).

The rate at which Ca^{2+} is released from the SR is assumed to satisfy an empirical equation defined by rising and falling exponentials (Baylor and Hollingworth, 2007): Release rate(t) = 0 if t < T, and is equal to

$$R \times \{1 - \exp[-(t - T)/\tau 1]\}^5 \times \exp[-(t - T)/\tau 2],$$
 (3)

if $t \ge T$.

The time-shift parameter T (value, 1–2 ms) simulates the delay between the external shock that generates the AP and the onset of Ca^{2^+} release; it is adjusted so that the rising phase of the simulated spatially averaged Δf_{CaD} waveform matches that of the measured Δf_{CaD} waveform. The amplitude parameter R is adjusted so that the peak of the simulated Δf_{CaD} waveform matches that of the measurement. The success of the simulation is evaluated by comparing the overall time course of the simulated and measured Δf_{CaD} waveforms.

Simulations that include Mg^{2+} binding to the troponin regulatory sites

To date, our simulations have assumed that the troponin regulatory sites bind Ca^{2+} specifically; i.e., without interference from Mg^{2+} (Potter and Gergely, 1975; Johnson et al., 1981). However, several reports in the literature indicate that Mg^{2+} , at physiological concentrations, may bind significantly to the regulatory sites. The work of Davis et al. (2002) is particularly striking in this regard. These

authors studied TnC from chicken skeletal muscle and demonstrated that the second Ca^{2+} regulatory site (EF-hand site II, counting from the N terminus) binds Mg^{2+} with a dissociation constant ($\text{K}_{\text{D,Mg}}$) of 2–4 mM, depending on measurement conditions; this value could be as low as 1–1.5 mM if cooperative binding of Ca^{2+} to the regulatory sites (Hill coefficient of 2) is considered in the analysis. The conclusion that Mg^{2+} can compete with Ca^{2+} for occupancy of the regulatory sties is strengthened by studies in skinned skeletal fibers that indicate that Mg^{2+} , at low millimolar concentrations, produces a right-shift in the tension–pCa curve (Godt and Lindley, 1982; Allen et al., 1992; Davis et al., 2002) and a right-shift in the Ca^{2+} -activated actomyosin ATPase curve (Morimoto, 1991).

Based on these findings, we have carried out some simulations (see Figs. 8, 10, and 11) that include competition between Mg²⁺ and Ca²⁺ for occupancy of the regulatory sites. For these simulations, the troponin reaction scheme shown in Fig. 3 was used, which is a simple extension of the scheme used previously for Ca²⁺'s reaction with the troponin regulatory sites in our compartment model for frog twitch fibers (Baylor et al., 2002; Hollingworth et al., 2006) and mouse fast-twitch fibers (Baylor and Hollingworth, 2007). The value chosen for $K_{D,Mg}$ (= k_3/k_{+3}) was 2 mM, which is in the range suggested by the work of Godt and Lindley (1982), Allen et al. (1992), and Davis et al. (2002). The on-rate constant (k_{+3}) was $6.0 \times$ 10⁴ M⁻¹s⁻¹ (16°C), which is the mean of the on-rate constants in our model for the reaction of Mg²⁺ with the metal-free sites on parvalbumin $(3.3 \times 10^4 \,\mathrm{M}^{-1} \mathrm{s}^{-1})$ and the $\mathrm{Ca^{2+}}$ pump $(8.7 \times 10^4 \,\mathrm{M}^{-1} \mathrm{s}^{-1})$. The off-rate constant (k_3) was 120 s^{-1} , calculated as the product of the dissociation constant and the on-rate constant.

Statistics

Student's two-tailed t test was used to test for differences between population mean values, with the significance level set at P < 0.05.

RESULTS

Fiber measurements

Fig. 4 shows an example of the tension response (lower-most trace) and the furaptra $\Delta F/F_R$ signal (middle trace) recorded from a mouse fast-twitch fiber (A) and a frog twitch fiber (B) stimulated by a single AP (16°C). The top trace in each panel shows Δf_{CaD} calculated from $\Delta F/F_R$

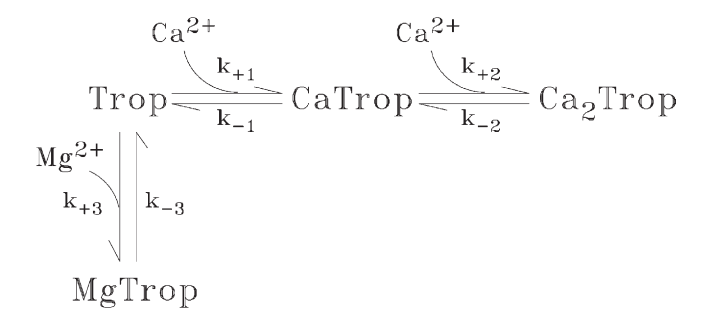


Figure 3. Four-state reaction scheme for the troponin regulatory sites in which Mg^{2+} competes with Ca^{2+} for binding to the metal-free state. The values of k_{+1} , k_{-1} , k_{+2} , and k_{-2} are $1.77 \times 10^8\,M^{-1}s^{-1}$, $1,544\,s^{-1}$, $0.885\times 10^8\,M^{-1}s^{-1}$, and $17.1\,s^{-1}$, respectively (16°C; Baylor and Hollingworth, 2007). In the simulations without Mg^{2+} competition (Figs. 5–7, 9, 10 A, and 11 A), the troponin reaction included only the Mg^{2+} -free states; with resting $[Ca^{2+}] = 50\,$ nM, the resting fractional occupancies are 0.993 (Trop), 0.006 (CaTrop), and 0.001 (Ca₂Trop). In the simulations of Figs. 8, 10 B, and 11 B, the values of k_{+3} and k_{-3} were $6\times 10^4\,M^{-1}s^{-1}$ and $120\,s^{-1}$, respectively ($K_{D,Mg} = 2\,$ mM). With resting $[Mg^{2+}] = 1\,$ mM, the resting fractional occupancies of the four states are 0.663 (Trop), 0.004 (CaTrop), 0.001 (Ca₂Trop), and 0.332 (MgTrop). Table 1 gives the (spatially averaged) troponin concentration.

with Eq. 1. The peak amplitude and time of peak of the Δf_{CaD} traces are similar in the two experiments (see figure legend), but the decay time course of Δf_{CaD} is slower in the frog fiber and the FDHM is consequently larger (12 vs. 5 ms).

Results were compiled from several experiments like those in Fig. 4 in which contamination of the Δf_{CaD} measurements with movement artifacts was very small or negligible (mouse, n=8; frog, n=7). In mice, the peak value of Δf_{CaD} was 0.157 ± 0.004 (mean \pm SEM); in frogs it was

 0.150 ± 0.012 . The FDHM values were 5.4 ± 0.5 ms and 10.1 ± 0.5 ms, respectively. The difference in peak values is not statistically significant (P > 0.05), whereas the difference in FDHMs is highly significant (P < 0.001). Although the mean diameters of the fibers selected for this comparison were significantly different (41 \pm 2 μ m for mouse and $53 \pm 4 \,\mu m$ for frog; P = 0.009), the difference in FDHM does not appear to be attributable to the difference in fiber diameter. If the comparison of FDHMs is restricted to the fibers with closely similar diameters, namely the six largest mouse fibers (diameter, $44 \pm 1 \mu m$) and the three smallest frog fibers (diameter, $44 \pm 2 \mu m$), a similar difference in FDHM is observed, 5.7 ± 0.5 ms versus 9.2 ± 0.4 ms, respectively (P = 0.003). Thus, the difference in FDHM appears to reflect some consistent difference in the underlying myoplasmic Ca²⁺ movements in the two fiber types.

Single-compartment (spatially averaged) modeling

In Fig. 5, the lowermost trace in each panel shows the averaged Δf_{CaD} signal obtained from the fibers discussed in the preceding section (A, mouse, n=8; B, frog, n=7). The upper traces in each panel show three spatially averaged estimates derived from the corresponding Δf_{CaD} trace: (a) $\Delta [Ca^{2+}]$, which was calculated with Eq. 2; (b) the total amount of SR Ca²⁺ release ($\Delta [Ca_T]$, with units referred to the myoplasmic water volume), which was estimated from $\Delta [Ca^{2+}]$ and the single-compartment (spatially averaged) version of the myoplasmic Ca²⁺ model (e.g., as calculated with the method of Baylor et al., 1983; and Baylor and Hollingworth, 1988, 2003); and (c) the rate of SR Ca²⁺ release. In each panel, the release rate with noise was calculated from the corresponding $\Delta [Ca_T]$

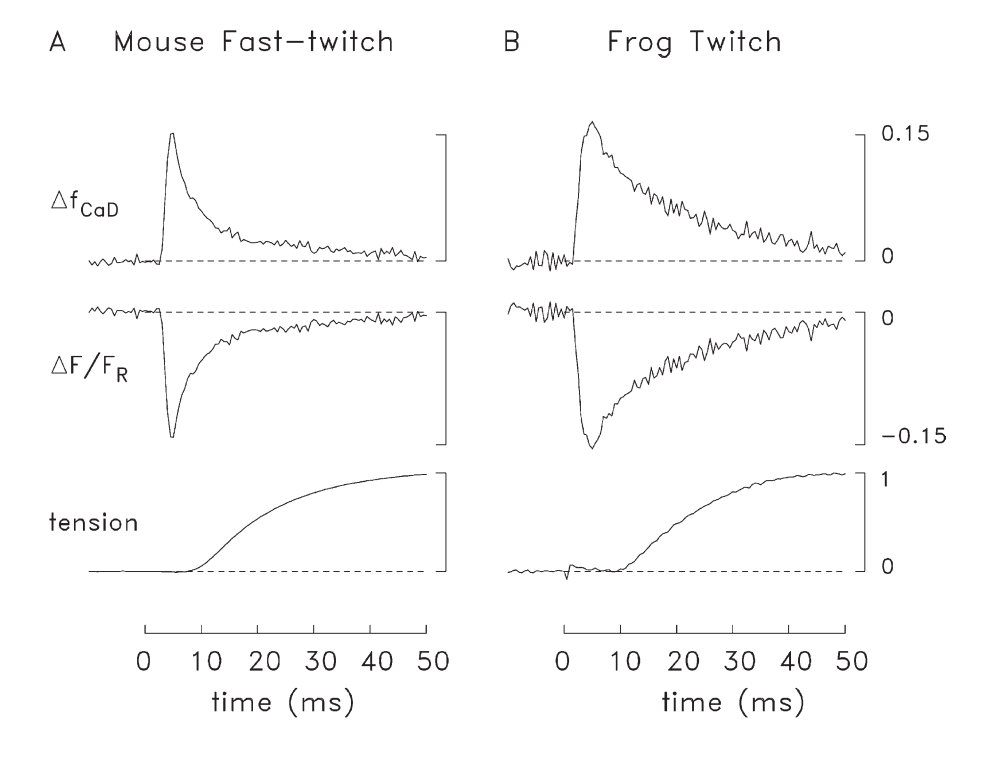


Figure 4. Representative experiments showing twitch tension (lowermost trace) and the furaptra fluorescence signal (upper traces) elicited by an AP in a mouse fast-twitch fiber (A) and a frog twitch fiber (B). Zero time marks the moment of the external shock; the tension trace in B has a small stimulus artifact. Peak amplitude, time of peak, and FDHM of Δf_{CaD} were 0.150, 5 ms, and 5 ms (A); and 0.164, 5 ms, and 12 ms (B). Fiber diameter, sarcomere spacing, and the number of sweeps averaged for each trace were 33 μm, 3.9 μm, and 2(A); and 54 μm, 3.8 μm, and 2, respectively (B). The labels and calibrations apply to both parts of the figure; the value 1.0 on the tension calibration corresponds to the peak of twitch tension.

trace as $(d/dt)\Delta[Ca_T]$; the noise-free trace (Fig. 5, broken lines) is a mathematical approximation of this release rate that satisfies Eq. 3 (see figure legend). Each noise-free trace was used as the initial release waveform in the multicompartment modeling described in the next section. The use of the output of the single-compartment simulations is thought to be a reasonable starting point for the multicompartment simulations. The goal of the latter is to yield an internally consistent explanation of the measured Δf_{CaD} signal in terms of the major underlying Ca movements taking place within a three-dimensional model of the fiber volume, such as is considered in our multicompartment simulations.

Multicompartment (spatially resolved) modeling

In Fig. 6, the upper traces in each panel show a comparison of simulated and measured Δf_{CaD} waveforms (A, mouse; B, frog). Each simulated Δf_{CaD} waveform (noise-free trace) was calculated with the multicompartment model (see Materials and methods) driven by a Ca²+ release rate having the functional form of Eq. 3. The release waveforms (Fig. 6, lower traces) are similar to the noise-free traces (broken lines) in Fig. 5, with the amplitude of each waveform adjusted so that the peak of each simulated Δf_{CaD} trace matched that of the corresponding measurement. In mouse fibers, the simulated and measured Δf_{CaD} traces are in good agreement (Fig. 6 A), whereas in frog fibers they are not (Fig. 6 B). The main discrepancy in frog is that the measured Δf_{CaD} decays

more slowly than the simulated Δf_{CaD} . Because the concentrations and properties of the myoplasmic Ca^{2+} buffers are thought to be similar in frog twitch fibers and mouse fast-twitch EDL fibers (e.g., Heizmann et al., 1982; Fink et al., 1986; Leberer and Pette, 1986; Godt and Maughan, 1988; Ecob-Prince and Leberer, 1989; Kushmerick et al., 1992), the discrepancy in Fig. 6 B suggests that the amount of SR Ca^{2+} release in frog fibers is larger, and has a slower overall time course, in the measurements than in the simulations.

Fig. 7 A shows a comparison for frog fibers like that in Fig. 6 B except that the simulated Ca²⁺ release rate is the sum of two components (broken lower traces), each of which satisfies the functional form of Eq. 3 (see legend). This release waveform has a slower final decay than that in Fig. 6 B and gives a somewhat larger total release (391) vs. 345 μM). Fig. 7 B shows the same comparison as that in Fig. 7 A but on a slower time base. The markedly improved overall agreement between the simulated and measured Δf_{CaD} waveforms in Fig. 7 A compared with Fig. 6 B supports the conclusion that this two-component release waveform is a reasonable approximation of the actual release waveform in frog fibers. This result contrasts with that in mouse fast-twitch fibers (Fig. 6 A), where the singlecomponent release function yielded a satisfactory multicompartment simulation.

It is perhaps surprising that, in the spatially resolved modeling of Fig. 7 A, an excellent simulation of the frog Δf_{CaD} waveform is obtained with a two-component Ca²⁺

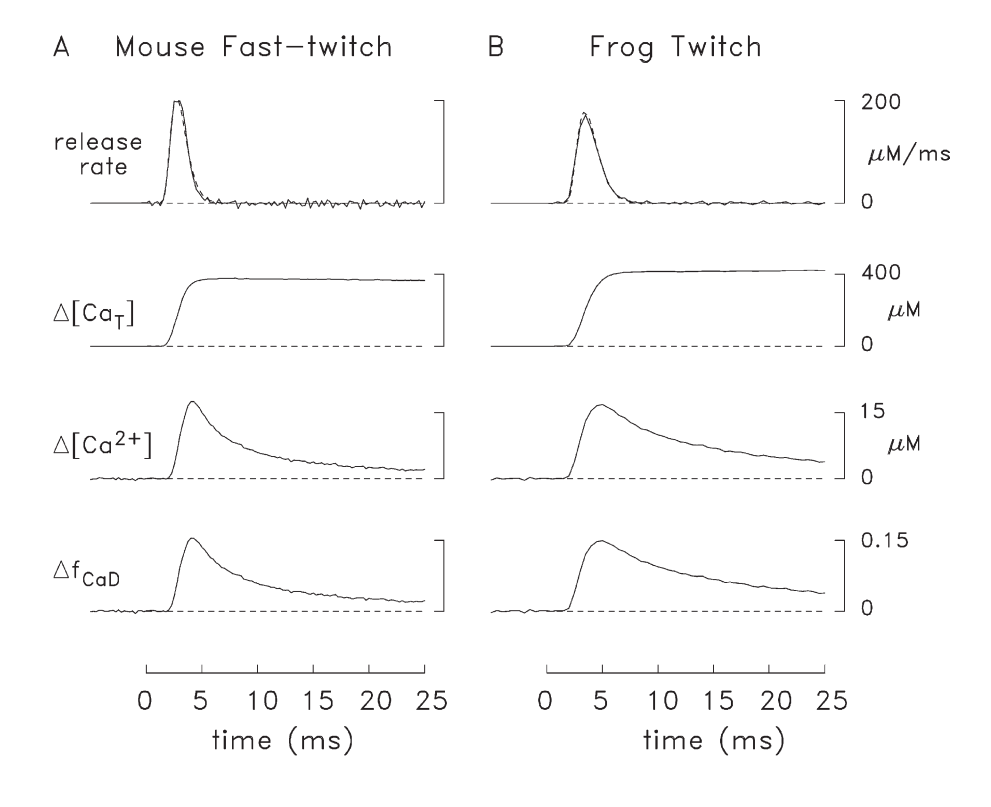


Figure 5. Comparison of single-compartment estimates of SR Ca²⁺ release in mouse and frog fibers stimulated by an AP. The lowermost trace in each panel shows an averaged furaptra Δf_{CaD} signal obtained from several experiments like that in Fig. 4 (A, mouse, n = 8; B, frog, n = 7); in all experiments, Δf_{CaD} appeared to be virtually free of movement artifacts. The peak, time of peak, and FDHM of the Δf_{CaD} traces are 0.154, 4.0 ms and 5.2 ms in A; and 0.149, 5.0 ms, and 10.3 ms in B, respectively. Each Δ [Ca²⁺] trace was calculated from Δ f_{CaD} with Eq. 2. The estimated total amount of released Ca^{2+} ($\Delta[Ca_T]$), which was calculated from Δ [Ca²⁺] with the singlecompartment version of the model, is equal to the sum of $\Delta[Ca^{2+}]$ and (not depicted) Δ [CaDye], Δ [CaATP], Δ [CaTrop], Δ [CaParv], Δ [CaPump], and Δ [CaPumped]. Peak Δ [Ca_T] is 380 μ M in A and 422 μM in B. The top traces show estimates of the rate of SR Ca2+ release. The traces with noise (peak value, $199 \,\mu\text{M/ms}$ in A and $172 \,\mu\text{M/ms}$ in B) are the derivative of the corresponding Δ [Ca_T] traces. The noise-free traces are mathematical representations of these

waveforms that satisfy Eq. 3. With these representations, the total release amount, and values of $\tau 1$ and $\tau 2$ are $380~\mu M$, 1.4 ms, and 0.55 ms in A; and $420~\mu M$, 1.75 ms, and 0.7 ms, respectively, in B. The FDHM of the release waveform is 1.7 ms in A and 2.2 ms in B.

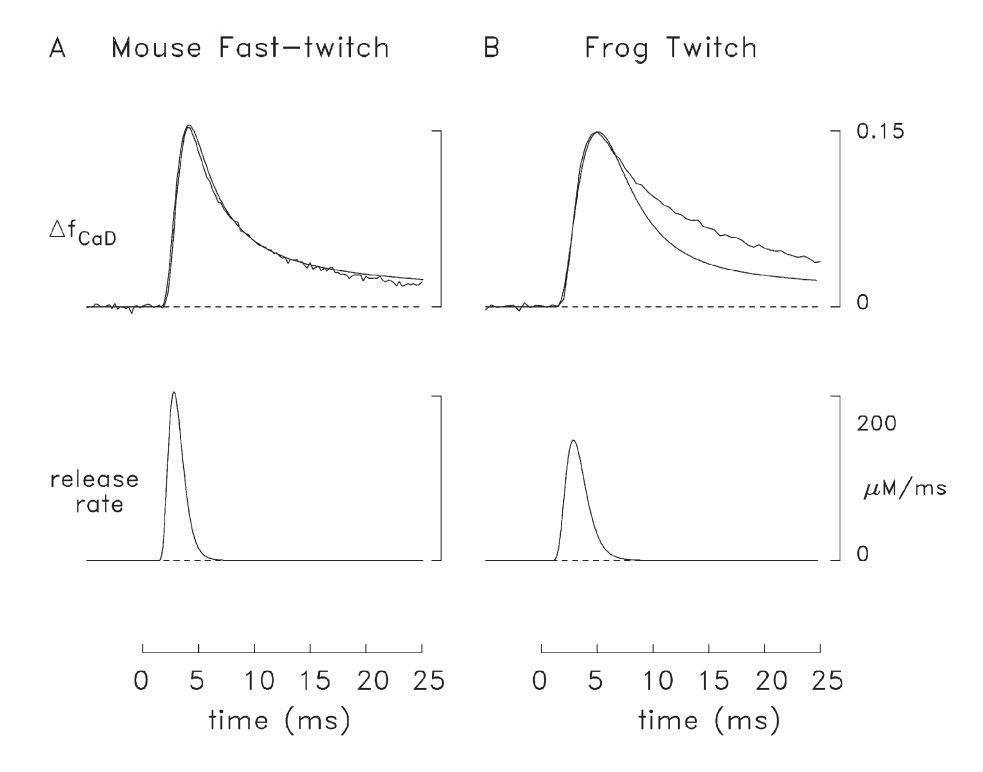
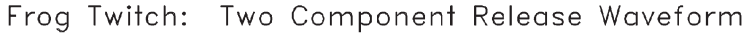


Figure 6. Comparison of multicompartment simulations in mouse and frog fibers. In both fiber types, the simulated SR release waveform has the functional form of Eq. 3; the parameter values are similar to those in the corresponding parts of Fig. 5 except that the total release amounts and values of $\tau 1$ and $\tau 2$ are 349 μM , 1.3 ms, and 0.5 ms (A); and 345 µM, 1.75 ms, and 0.7 ms, respectively (B). With these values, the peak of each simulated Δf_{CaD} waveform matches that of the corresponding measurement. The FDHM of the simulated Δf_{CaD} waveform is 5.1 ms in A and 6.7 ms in B. The peak value, time of peak, and FDHM of the release waveforms are 205 μM/ms, 2.8 ms, and 1.6 ms (A); and 144 μ M/ms, 2.9 ms, and 2.2 ms, respectively (B).

release function even though the Ca²⁺ release waveform estimated in the spatially averaged modeling of Fig. 5 B has no discernible second component. This situation arises because of subtle differences inherent in the spatially averaged versus spatially resolved modeling approaches. For example, if the simulated Δf_{CaD} waveform from the spatially resolved model (Fig. 7 A) is used as the starting point in the spatially averaged model, a second release component, as expected, is not resolved.

Possible competition between Mg²⁺ and Ca²⁺ for the troponin regulatory sites

Several reports in the literature indicate that Mg²⁺ may compete with Ca²⁺ for occupancy of the troponin regulatory sites (see Introduction and Materials and methods), a possibility not considered in the previous modeling. To examine how such Mg²⁺ competition might impact the simulations, the reaction scheme shown in Fig. 3 was substituted for our usual troponin scheme; the concentration



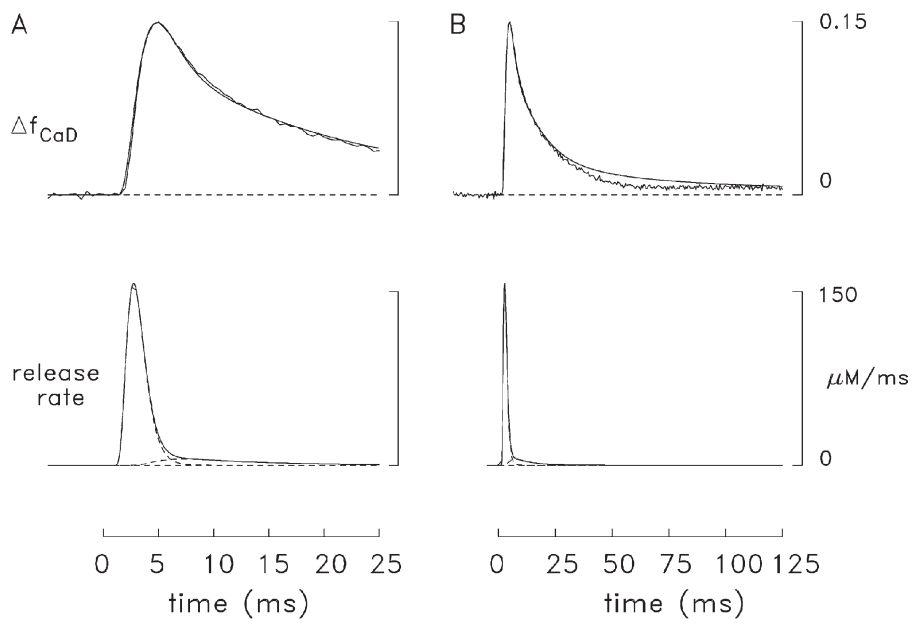


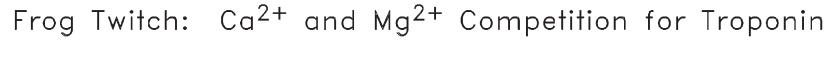
Figure 7. Comparison of simulated and measured frog Δf_{CaD} signals. (A) Comparison like that in Fig. 6 B except that the theoretical release function is the sum of two components (broken traces), each of which has the functional form of Eq. 3. The values of release amount, $\tau 1$, and $\tau 2$ are 335 μM , 1.5 ms, and 0.65 ms (first component); and 56 µM, 1.7 ms, and 7 ms, respectively (second component); the onset of the second component is assumed to lag that of the first component by 1 ms (T in Eq. 3 is 1 ms for the first component and 2 ms for the second). The peak value, time of peak, and FDHM of the composite release waveform are 157 μ M/ms, 2.7 ms, and 2.0 ms. (B) Same traces as in A but on a fivefold slower time base.

of myoplasmic free [Mg²⁺] in the model was, as usual, 1 mM and constant. Fig. 8 shows results of a multicompartment frog simulation with this change. As in Fig. 7, a two-component release function was used (lowermost traces; see legend of Fig. 8), and good agreement was again observed between the simulated and measured Δf_{CaD} waveforms (middle traces). As expected, the spatially averaged change in the concentration of troponin molecules whose regulatory sites are both occupied with Ca^{2+} (Fig. 8, $\Delta[Ca_2Trop]$, upper traces), which is the troponin state that is likely to be functionally important for activation of the fiber's contractile response, has a smaller peak value in this simulation (99 µM, continuous trace) than in the simulation of Fig. 7 (112 µM, broken trace) and a later time of peak (20 vs. 15 ms). The estimated amount of SR Ca²⁺ release is slightly smaller in the simulation of Fig. 8 than in Fig. 7 (374 vs. 391 µM) and the fractional amounts of the first and second release components differ modestly (0.76 and 0.24 in Fig. 8 vs. 0.86 and 0.14 in Fig. 7). Overall, the Ca²⁺ release waveform estimated in the modeling is not strongly affected by use of a troponin reaction with a moderate sensitivity to Mg²⁺.

Effects of faster reaction rates between Ca²⁺ and troponin As noted in the preceding section, the overall time course with which Ca²⁺ binds to troponin is slower in the simulation in which Mg²⁺ is permitted to bind to the regulatory sites, and the estimated proportion of the released Ca²⁺ due to the second release component is increased somewhat. One would therefore expect that the fractional amount of release due to the second component would be reduced in a simulation in which

Ca²⁺ reacted more rapidly with the regulatory sites. As noted previously (Baylor et al., 2002; Hollingworth et al., 2006), the reaction scheme between Ca²⁺ and troponin in our model is based on the cooperative binding of two Ca²⁺ ions to each troponin molecule (see Fig. 3 and legend). The limiting rate constant for the dissociation of Ca^{2+} from troponin ($k_{-2} = 17.1 \text{ s}^{-1}$; 16°C) was chosen to be consistent with the experimental findings of Davis et al. (Davis, J.P., S.B. Tikunova, D.R. Swartz, and J.A. Rall. 2004. Biophysical Society Annual Meeting, Abstr. 1135). With this scheme and rate constants, good agreement was observed between the properties of simulated and measured Ca²⁺ sparks in frog intact fibers (measured with fluo-3; Baylor et al., 2002). This suggests that the Ca²⁺-troponin reaction is reasonably well modeled, as troponin is the dominant myoplasmic Ca²⁺ buffer on a fast time scale and the simulated spark properties are sensitive to the troponin reaction rate constants. Nevertheless, because troponin's reaction with Ca²⁺ is expected to have a significant influence in shaping the furaptra Δf_{CaD} waveform elicited by an AP and thus on the estimated amount of SR Ca²⁺ release, it was of interest to consider how the conclusions of the modeling would be affected if the actual Ca²⁺-troponin rate constants are larger than the values assumed in the simulations of Figs. 5–8.

To investigate this question, a frog simulation like that in Fig. 7 was carried out with the values of the four reaction rate constants involving Ca²⁺ and troponin (see Fig. 3 and legend) increased twofold. This change does not affect the dissociation constants of the Ca²⁺–troponin reactions and thus the steady-state value of [Ca²⁺] that gives half-occupancy of the troponin sites with Ca²⁺,



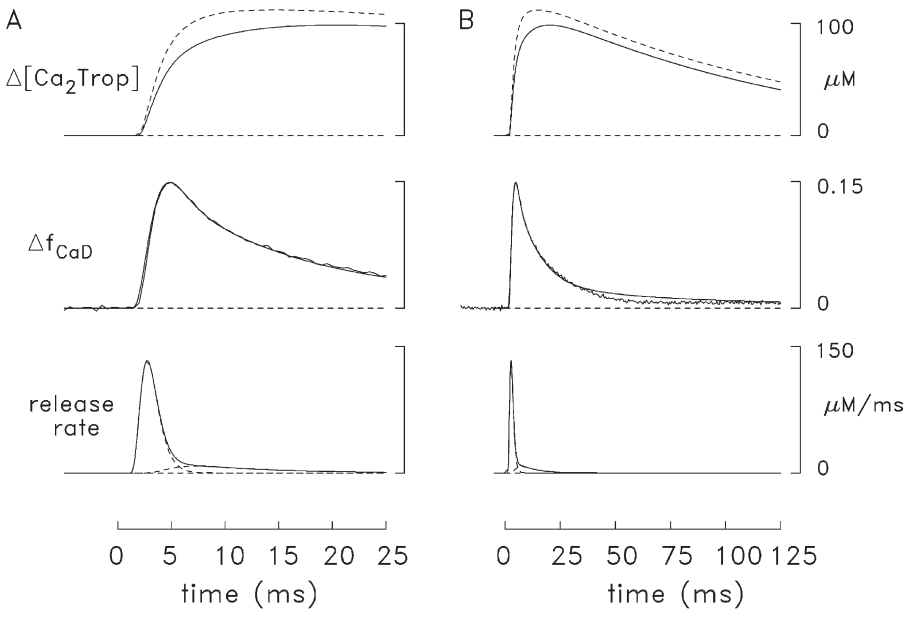


Figure 8. Results of a simulation like that in Fig. 7 except that the modeled troponin reaction included competition between Mg²⁺ and Ca²⁺ (see Fig. 3). In each panel (A, faster time base; B, slower time base), the superimposed traces at the top show simulated changes in the spatially averaged concentration of the doubly occupied Ca²⁺-troponin state (rightmost state in Fig. 3), which were averaged over the nine troponincontaining compartments (see Fig. 2). The continuous trace is from this simulation; the broken trace is from the simulation of Fig. 7. For this simulation, the release amounts, $\tau 1$, and $\tau 2$ are 284 μM, 1.5 ms, and 0.65 ms (first component); and 90 µM, 1.7 ms, and 7 ms, respectively (second component). The peak value, time of peak, and FDHM of the composite release waveform are $133~\mu M/ms,\,2.7~ms,$ and 2.0~ms.

1.3 µM. In this simulation (not depicted), good agreement between the simulated and measured Δf_{CaD} traces was again observed (similar to that in Figs. 7 and 8). The estimated total concentration of released Ca²⁺, 394 µM, is essentially identical to that in the simulation of Fig. 7, whereas the fractional amounts assigned to the first and second release components (0.88 and 0.12) differ slightly from that in the simulation of Fig. 7 (0.86 and 0.14). Overall, the Ca²⁺ release waveform estimated with the multicompartment model is not strongly affected by use of a troponin reaction scheme, with substantially increased rate constants between Ca²⁺ and the regulatory sites. Thus, simulations carried out under the assumption that Ca²⁺ binds to troponin more rapidly (this section) or more slowly (previous section) than is assumed in our standard model do not explain the observation of a slower decay of Δf_{CaD} in frog fibers compared with mouse EDL fibers. This result adds support to the interpretation that the slow decay of Δf_{CaD} in frog fibers is caused by an extra component of release that continues for some milliseconds after decline of the major portion of the release and not by an error in the choice of rate constants for the Ca²⁺-troponin reaction.

Effects of changes in other model parameters on the simulation of Δf_{CaD} in frog fibers

Because parvalbumin, like troponin, binds a substantial amount of the released Ca²⁺ on the fast time scale of the measurements, simulations were also carried out with the multicompartment model to investigate whether the use of altered parameter values for parvalbumin in combination with the single-component Ca²⁺ release waveform would yield a satisfactory simulation of the frog Δf_{CaD} signal. The alterations considered included reductions in (a) the concentration of parvalbumin and (b) the rate constants for the reactions of Ca²⁺ and Mg²⁺ with parvalbumin. In both cases, parvalbumin should capture less Ca²⁺ than in the simulation with the standard parameter values, which should slow the decay of Δ [Ca²⁺] from its peak and produce better agreement between the simulated and measured Δf_{CaD} waveforms. Results based on the first possibility are shown in the top panels of Fig. 9, in which the concentration of metal sites on parvalbumin was reduced twofold, from 1,500 to 750 μM (a change that is larger than reasonable). The time course of the single-component Ca²⁺ release waveform used to drive the simulation was identical to that in Fig. 6 B; as usual, the amplitude of the release flux was adjusted so that the peak of the simulated spatially averaged Δf_{CaD} waveform matched that of the measurement. Fig. 9 A reveals that, in comparison with the simulation of Fig. 6 B, there is, as expected, improved agreement with the measurement during the period 10-25 ms after stimulation; however, the later rising phase, time of peak, and early falling phase of the simulated waveform are in less-satisfactory agreement with the measurement

than in the simulation of Fig. 6 B. In addition, Fig. 9 B reveals that the improved agreement in Fig. 9 A during the period 10-25 ms is not maintained on a time scale of 125 ms; during the period of 40–125 ms, a substantial discrepancy is observed between the simulated and the measured waveforms, which is greater than that seen in the simulations of Figs. 7 B and 8 B (both of which used a two-component release waveform). Results similar to those in Fig. 9 (A and B; not depicted) were observed if the parvalbumin site concentration was restored to its original value (1,500 μM), and the on- and off-rate constants for the reactions of Ca²⁺ and Mg²⁺ with parvalbumin were reduced twofold. Overall, these perturbations indicate that, with a single-component release function, simulations with the altered parameter choices for parvalbumin do not yield satisfactory agreement between the simulated and measured Δf_{CaD} waveforms.

Simulations with the single-component Ca²⁺ release function that included changes in several other modeling parameters were also explored, including changes in concentration of the SR Ca²⁺ pump molecules, changes in the rate constants with which Ca2+ and Mg2+ react with the Ca²⁺ pump, and changes in the concentration of ATP. When the concentration of Ca²⁺ pump molecules was set to half the normal value or when the reaction rate constants of the pump with Ca2+ and Mg2+ were reduced twofold, the simulated and measured Δf_{CaD} waveforms revealed substantial discrepancies (not depicted), similar to the discrepancies shown in Fig. 9 (A and B). When the ATP concentration was increased from 8 to 15 mM, better agreement between the simulated and measured Δf_{CaD} waveforms was observed (Fig. 9, bottom panels) than was seen with the other individual modeling changes that were investigated. However, even when this unreasonably large concentration of ATP was used in the model, the overall agreement between the simulated and measured Δf_{CaD} waveforms in Fig. 9 (C and D) is not as satisfactory as that in Figs. 7 and 8, where better agreement is observed in the later rising phase, time of peak, and early falling phase of the Δf_{CaD} waveforms (compare Fig. 9 C vs. Figs. 7 A and 8 A) and also in the late return toward baseline (40–125 ms; Fig. 9 D vs. Figs. 7 B and 8 B). Overall, the additional simulations described in this section indicate that the most straightforward modeling change that achieves a satisfactory simulation of the measured Δf_{CaD} signal in frog fibers is the addition of a small second component to the SR Ca²⁺ release waveform.

Functional importance of the second release component in frog fibers

As noted in Fig. 2, the site of SR Ca²⁺ release differs in the mouse and frog models, being positioned near the middle of the thin filament in the mouse model and near the z-line end of the thin filament in the frog model. The effect on the simulations due to this positional difference was considered previously in our mouse modeling carried

out at a normal sarcomere length (2.4 µm; Baylor and Hollingworth, 2007). The principal effect noted was that, for the estimated Ca²⁺ release waveform elicited by an AP (lower trace in Fig. 6 A), the troponin molecules at the end of the thin filament closer to the m-line have a noticeably smaller Ca²⁺ occupancy in the case of the frog release location compared with the mouse location (mean peak of the Ca₂Trop state, 68% vs. 81% of maximum, respectively). This difference would be expected to have a significant effect on the amplitude of the twitch because this region of the thin filament is within reach of the myosin cross-bridges at most working sarcomere lengths. Thus, the mammalian release location has the functional advantage that, for a given release waveform, the released Ca²⁺ is more effective at activating the myofilaments. Because frog fibers do not have this advantage, it is necessary to release more Ca²⁺ to achieve the same degree of contractile activation.

Fig. 10 examines this point further by considering what compartment differences in $\Delta[\text{Ca}^{2+}]$ and $\Delta[\text{Ca}_2\text{Trop}]$ occur if SR Ca²⁺ release in a frog fiber were to involve just the first release component of the two-component release waveform. The continuous traces in Fig. 10 (A and B) are taken from the simulations of Figs. 7 and 8, respectively (two-component release waveform), whereas the broken traces show the corresponding results if just the first release component in these simulations is used. The three $\Delta[Ca^{2+}]$ traces of similar type (continuous or broken) show radially averaged changes in the free Ca²⁺ concentration at three longitudinal locations at increasing distances from the z-line (largest peak value, mean of the three radial compartments nearest the z-line; intermediate peak value, mean of the three radial compartments in the middle of the thin filament; smallest peak value, mean of the three radial compartments at the end of the thin filament closer to the m-line; see Fig. 2). The three

 Δ [Ca₂Trop] traces of similar type (broken or continuous) show the corresponding changes in the concentration of the Ca₂Trop state of troponin. In each comparison, the peak value of Δ [Ca₂Trop] averaged for the three troponin-containing compartments nearest the m-line is noticeably smaller in the simulation with one release component than with two. In Fig. 10 A, the peak values of these traces are 91 and 106 µM, respectively, which correspond to 76% and 89% of maximum; in Fig. 10 B, the corresponding values are 66 and 89 µM, which correspond to 56% and 75% of maximum. Overall, these percentage comparisons are similar to those mentioned in the preceding paragraph (68 vs. 81%), which apply if results for the mouse Ca2+ release waveform are compared at the frog and mouse release locations (simulation without Mg²⁺ competition for troponin; half-sarcomere length = 1.2 μm). These comparisons indicate that having both the first and second components of the Ca²⁺ release waveform at the frog release location (a) substantially increases Ca²⁺'s occupancy of the troponin molecules nearest the m line, and (b) is functionally similar to having only the first release component at the mouse release location.

Simulations were also carried out with the short sarcomere model (half-sarcomere length = 1.2 μ m) to examine the functional significance of the frog second release component in relation to the two different locations of SR Ca²⁺ release. The endpoint evaluated in these simulations was again the peak percentage of troponin molecules in the troponin compartments nearest the m-line that are in the Ca₂Trop state. If the mouse release waveform of Fig. 6 A was moved to the z-line end of the thin filament, these percentages were 68% without addition of the frog second release component of Fig. 7 and 85% with addition of this component. Conversely, if the first component of the frog release waveform of Fig. 7 was

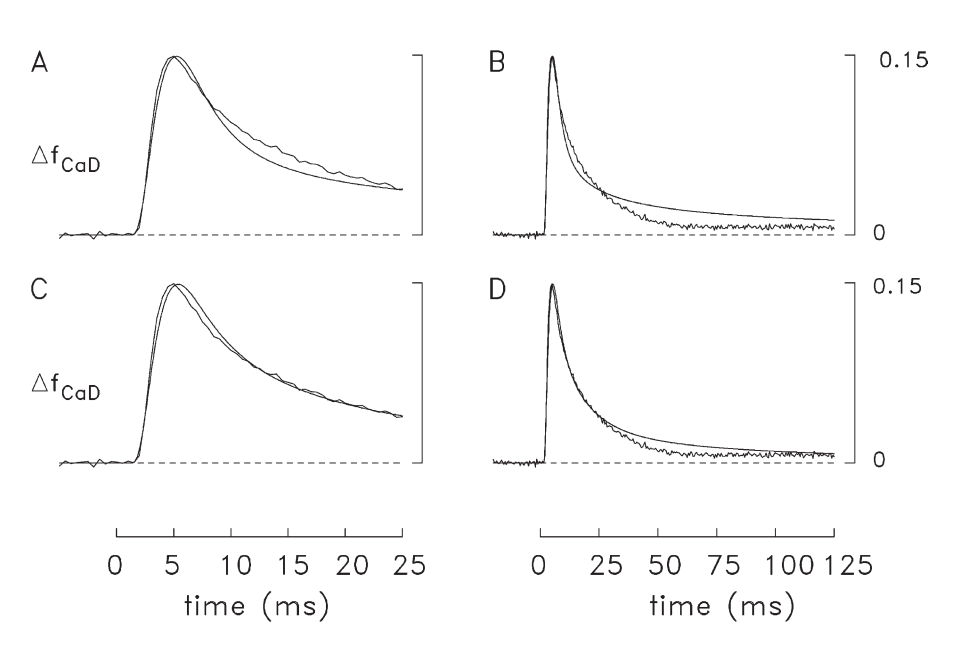


Figure 9. Results of frog simulations with a single-component Ca2+ release waveform and changes in parameter values for parvalbumin and ATP. (A) Comparison like that in Fig. 7 but with the concentration of parvalbumin sites reduced from 1,500 to 750 µM. The values of release amount, $\tau 1$, and τ 2 are 317 μ M, 1.75 ms, and 0.7 ms, respectively. The FDHM of the simulated Δf_{CaD} waveform is 8.3 ms. (B) Same traces as in A but on a fivefold slower time base. (C and D). Comparison like that in Fig. 7 but with the concentration of ATP increased from 8 to 15 mM. The values of release amount, 71, and τ2 are 399 μM, 1.7 ms, and 0.7 ms, respectively. The FDHM of the simulated Δf_{CaD} waveform is 10.1 ms.

moved to the middle of the thin filament, these percentages were 76% without addition of the second release component and 87% with addition of the second component. These simulations at a physiological sarcomere length confirm the functional advantage of the second component of release in frog fibers, as inferred in the preceding paragraph in the simulations at long sarcomere length.

Measurements and simulations of Δf_{CaD} in response to a brief high-frequency train of APs

Furaptra's Δf_{CaD} signal was also measured in several frog fibers that were stimulated to give 10 APs at 100 Hz. In five such experiments, the fibers were well immobilized and movement artifacts in the ΔF traces appeared to be small or negligible. The averaged Δf_{CaD} signal from these fibers is shown in both panels of Fig. 11 (traces with noise at the top). This measurement was simulated with the two approaches used in Figs. 7 and 8; i.e., with a twocomponent release function both without and with competition between Mg²⁺ and Ca²⁺ for the troponin regulatory sites. The other traces in Fig. 11 summarize the results of these simulations. The lowermost trace in each part shows the release waveform used to drive the simulation. Each AP in the train was assumed to elicit a two-component release waveform whose functional form matched that in Figs. 7 and 8, respectively (see legend of Fig. 11); the amplitude of each AP-evoked release of Ca2+ was adjusted in the usual way; i.e., so that each individual peak of Δf_{CaD} in the simulated Δf_{CaD} waveform matched the corresponding peak in the measurement. The second and third traces in each panel show two simulated Δ [Ca²⁺] waveforms. The one of larger amplitude is Δ [Ca²⁺] in the Ca²⁺ release compartment (the outermost compartment nearest the z-line; Fig. 2), where, in response to the first AP, Δ [Ca²⁺] reaches a peak of 90–100 μM and the subsequent peaks vary between ${\sim}45$ and $\sim 25 \,\mu\text{M}$. The smaller $\Delta [\text{Ca}^{2+}]$ trace is spatially averaged $\Delta[Ca^{2+}]$; here, peak amplitudes during the train vary between \sim 14 and \sim 19 μ M, and the shape of this waveform differs considerably from that of Δ [Ca²⁺] in the release compartment. The top traces in each panel show that there is good agreement between the simulated and measured Δf_{CaD} waveforms. In Fig. 11 A, the simulated amount of Ca²⁺ release caused by the first AP is \sim 377 µM, and the subsequent releases, considered as a percentage of the first release, vary from \sim 22% to \sim 10%. The corresponding values in Fig. 11 B are 343 μ M, 29%, and 11%, respectively. The large reductions in release that occur with the second and subsequent APs are likely caused by the process of Ca²⁺ inactivation of Ca^{2+} release, in which the $\Delta[Ca^{2+}]$ elicited by a prior AP feeds back in a negative fashion to inhibit the amount of Ca²⁺ released by the later APs in the train (see Discussion).

DISCUSSION

In frog twitch fibers activated by an AP, the amplitude of the furaptra Δf_{CaD} signal is similar to that in mouse fast-twitch EDL fibers but the decay of Δf_{CaD} is slower. The conditions for measurement of the Δf_{CaD} signals in the two fiber types were essentially identical, including the use of dissected intact fibers (single fibers for frog, small fiber bundles for mouse), the temperature (16°C), the mean sarcomere length of the fibers (3.7 \pm 0.1 μm in both

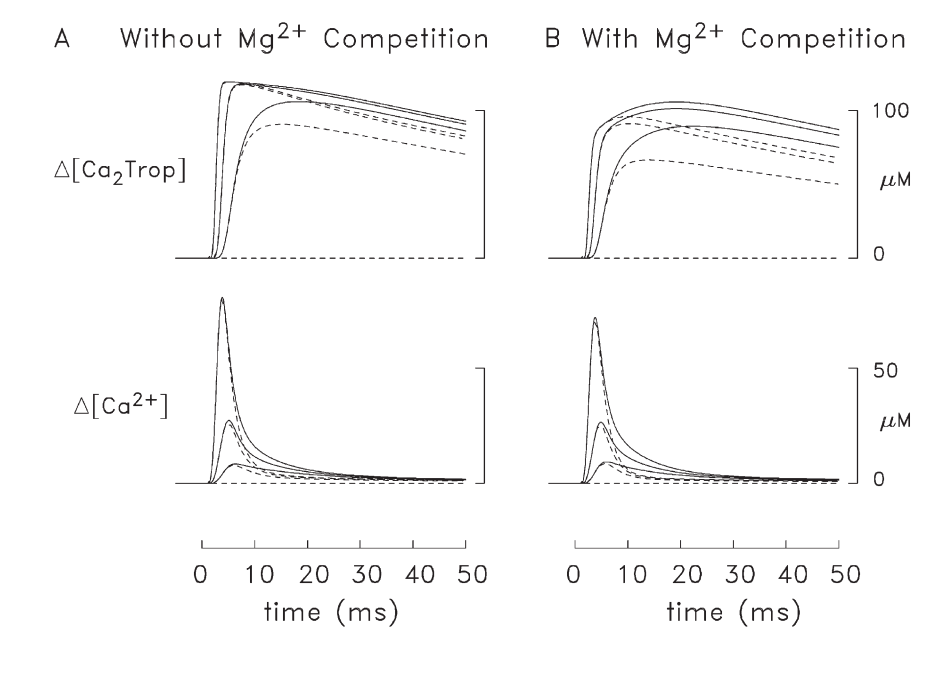


Figure 10. Differences in $\Delta [Ca^{2+}]$ and Δ [Ca₂Trop] waveforms in frog simulations that included both components of the release function (continuous traces) and only the first component of the release function (broken traces). In A, the troponin reaction did not include Mg²⁺ competition (simulated with the release function from Fig. 7); in B, the reaction in Fig. 3 was used (simulated with the release function from Fig. 8). Among any three traces of similar type (broken or continuous), the traces with the largest, intermediate, and smallest peak values are the averages, respectively, of the changes in the three radial compartments adjacent to the z-line, the three radial compartments in the middle of the thin filament, and the three radial compartments at the m-line end of the thin filament (compare with Fig. 2). The length of the half-sarcomere in the simulation was 2.0 μm (as in Figs. 6–9).

studies), the mean diameter of the fibers (53 \pm 4 μ m for frog, n = 7; 41 ± 2 µm for mouse, n = 8), and the myoplasmic concentration of furaptra (~0.1 mM). Thus, we are confident that the comparison of the experimental properties of Δf_{CaD} in the two fiber types is valid. Because the concentrations and properties of the myoplasmic Ca²⁺ buffers appear to be similar in these fiber types (e.g., Heizmann et al., 1982; Fink et al., 1986; Leberer and Pette, 1986; Godt and Maughan, 1988; Ecob-Prince and Leberer, 1989; Kushmerick et al., 1992), the slower decay of Δf_{CaD} in frog fibers suggests that the overall time course of Ca²⁺ release is slower, and the release amount is larger, in frog than in mouse fibers. Multicompartment modeling reveals that the frog Δf_{CaD} signal elicited by an AP is well simulated under the assumption that the Ca²⁺ release waveform is the sum of two kinetic components, a larger and faster one (fractional release amount, ~ 0.8 : FDHM, \sim 2 ms), and a smaller and slower one (fractional release amount, \sim 0.2; FDHM, \sim 9 ms). The FDHM of the faster component is similar to that of the entire SR Ca²⁺ release waveform estimated previously in mouse fast-twitch fibers, 1.6 ms (Baylor and Hollingworth, 2007), and in mouse slow-twitch fibers, 1.7 ms (Hollingworth et al., 2012).

Comparisons with measurements and proposals in the literature

The mechanism of activation of RyRs is hypothesized to differ significantly in mammalian and amphibian fibers. In mammals, the junctional RyRs that are apposed by DHPR tetrads (see Introduction and Fig. 1) are thought to be under conformational control of the overlying DHPRs via a direct protein-protein interaction (Schneider and Chandler, 1973; Beam and Horowicz, 2004), a mechanism sometimes called voltage-induced Ca²⁺ release (VICR). Exactly how control of the junctional RyRs that are not apposed by DHPR tetrads is achieved is an open question. Possibilities include: (a) Ca²⁺-induced Ca²⁺ release (CICR; e.g., Ríos and Pizarro, 1988; Stern et al., 1997), in which Ca²⁺ ions released from RyRs apposed by tetrads reach the nonapposed RyRs by diffusion and activate them via a ligand interaction; and (b) coupledgating (Marx et al., 1998), in which a conformational change in an activated RyR apposed by a tetrad activates an adjacent (nonapposed) RyR via a protein-protein interaction. In amphibians, the parajunctional RyRs appear to be too far removed from the junction to be activatable by either VICR or coupled gating, but, as proposed by Felder and Franzini-Armstrong (2002), they

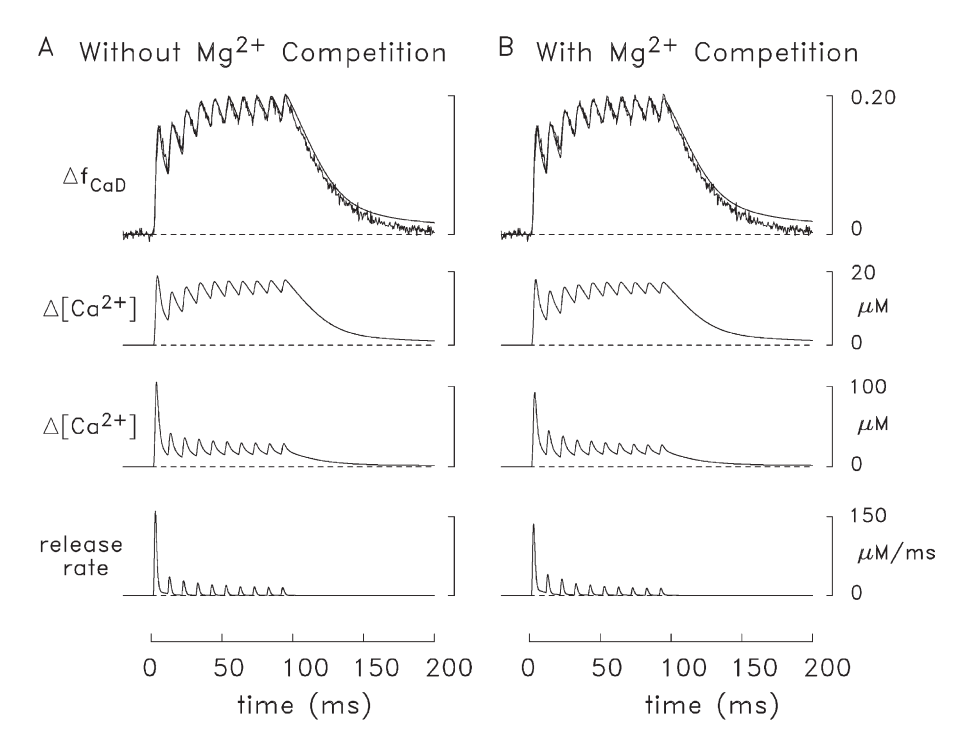


Figure 11. Comparison of simulated and measured frog Δf_{CaD} signals elicited by 10 APs at 100 Hz. In A, the simulated troponin reaction did not include Mg²⁺ competition; in B, the reaction in Fig. 3 was used. The lowermost trace in each panel shows the Ca2+ release waveform used to drive the simulation. The next trace shows simulated Δ [Ca²⁺] in the release compartment (see Fig. 2), and the third trace is the simulated spatially averaged $\Delta[\text{Ca}^{2+}]$ (i.e., the average of the $\Delta[Ca^{2+}]$ waveforms in all 18 compartments of the model). The top traces compare the simulated and measured Δf_{CaD} signals (noise-free and noisy traces, respectively). The measured Δf_{CaD} signal (which is shown in both panels) was averaged from five fibers in which contamination of the fluorescence signal with movement artifacts was very small or negligible. The mean diameter and mean sarcomere length of these fibers were 54 ± $3 \mu m \text{ (mean } \pm \text{ SEM)} \text{ and } 3.7 \pm 0.1 \mu m,$ respectively. The release functions for the simulations in A and B were based

on the two-component release functions in Figs. 7 and 8, respectively. For convenience in the calculation, it was assumed that the onset of each subsequent release extinguished any residual release elicited by the preceding APs and that the relative amplitudes of the two release components remain unchanged with the second and subsequent releases, measurements in frog cut fibers indicate that virtually all of the Ca^{2+} release channels (>90%) are subject to Ca^{2+} inactivation of Ca^{2+} release (Jong et al., 1995). The simulated release due to the first AP continued to 10.6 ms, the time at which the second release became significant. The second and subsequent releases were shifted in successive 10-ms increments and their amplitudes scaled down appropriately. In A, the amount of Ca^{2+} released with the first AP is 377 μ M and the amounts of the subsequent releases, expressed as a percentage of this amount, are 21.8, 17.5, 14.9, 12.6, 11.7, 10.4, 10.2, 9.5, and 10.0%, respectively. In B, the corresponding values are 343 μ M and 29.2, 22.8, 16.4, 14.7, 12.7, 11.7, 10.8, 10.1, and 11.2%.

might be activated by CICR via the Ca²⁺ ions released, at least initially, from junctional RyRs. The presence of parajunctional RyRs in amphibian fibers is consistent with proposals in the literature that CICR is mechanistically significant in amphibian fibers (Ríos and Pizarro, 1988; Jacquemond et al., 1991; Pizarro et al., 1992; O'Brien et al., 1995; Sutko and Airey, 1996; Klein et al., 1996; Pape and Carrier, 1998; González et al., 2000; Pape et al., 2002).

Our description of two release components in frog fibers and one component in mouse fibers is qualitatively consistent with the literature proposals that SR Ca²⁺ release in (adult) amphibian fibers depends on both VICR and CICR, whereas that in (adult) mammalian fibers is due primarily to VICR. It is also qualitatively consistent with the finding that amphibian RyRs are comprised of approximately equal amounts of two isoforms, RyRα and RyRβ, whereas the RyRs in (most) mammalian fibers consist of one main isoform, RyR1 (see Introduction). An obvious interpretation of our results (Figs. 7, 8, and 11) is that the modeled first component of the frog release waveform reflects activity of junctional RyRs, perhaps exclusively activated by VICR, whereas the second component reflects activity of parajunctional RyRs, perhaps exclusively activated by CICR.

Functional significance of the second release component

As mentioned in Results (Fig. 10 and associated text), our simulations in frog fibers indicate that the peak change in concentration of the Ca₂Trop state of the troponin molecules that are most distant from the z-line is substantially increased by the presence of the second component of release. Activation of these troponin molecules is likely to be functionally quite important at most working sarcomere lengths, and inclusion of the second release component in the frog model reveals a degree of troponin activation that is similar to that which occurs in the mouse model, which does not include a second release component and where the triadic junctions are located more centrally along the length of the thin filament. One may therefore speculate that two design strategies have evolved among adult vertebrate twitch fibers to achieve a high degree of troponin activation along the entire length of the thin filament in response to an AP: (a) a Ca²⁺ release location near the z-line with extra Ca²⁺ release caused by the second release component, and (b) a release location near the middle of the thin filament with less Ca²⁺ release; i.e., with that due just to a fast release waveform. (This speculation is similar to one proposed by E. Stephenson; see the Discussion of Shirokova et al., 1996.) The first strategy is represented by most fibers of amphibians, fish, and birds, which have both RyRα and RyRβ, and likely have both junctional and parajunctional RyRs (which, if the speculation of Felder and Franzini-Armstrong [2002] is correct, correspond to RyRα and RyRβ, respectively). The second strategy is represented by most fibers of mammals as well as those of many reptiles (e.g., lizards and snakes; O'Brien et al., 1995), which have only one RyR isoform (namely, RyR1 or its equivalent) and may have only junctional RyRs. An exception to the z-line location of the triadic junctions in fish muscle occurs in the superfast fibers of the toadfish swim bladder muscle, whose triadic junctions are located near the middle of the thin filament. Interestingly, swim bladder fibers have only a single RyR isoform (O'Brien et al., 1993), lack parajunctional RyRs (Felder and Franzini-Armstrong, 2002), and have a brief Ca²⁺ release waveform (Harwood et al., 2011), i.e., they adhere to the second design strategy. In summary, we speculate that the (most common) function of the parajunctional RyRs in adult vertebrate fibers is to permit a modest increase in the amount of SR Ca²⁺ release with an AP when triads are located near the z-line; this compensates for the smaller activation of troponin that would otherwise occur given that the z-line location for Ca2+ release is inherently less favorable for complete activation of the myofilaments (Fig. 10 and associated text). In terms of the peak occupancy of troponin with Ca²⁺, the benefit of this extra release would likely apply primarily to the activation of troponin in response to a single AP or a series of APs that do not occur in close succession, because, with a high-frequency stimulus, most of the regulatory sites on troponin would likely be bound with Ca²⁺ by the time of the second or third AP in the stimulus train. Even with a high-frequency stimulus, some benefit may arise from the second component in having a more synchronous activation of troponin along the length of the thin filament.

Other experimental approaches and alternative interpretations

Although we believe that the presence of a second release component is the most likely explanation of the slow decay of the furaptra Δf_{CaD} waveform that we have measured in frog fibers, it should be acknowledged that the evidence for this is indirect, as it relies on inferences based on a complex multicompartment kinetic model whose parameters are not all known with a high degree of certainty. In addition, the basic measurement of Δf_{CaD} is a spatially averaged one in which fluorescence is collected from a \sim 300-µm fiber length and the full fiber width, the volume of which is many-fold larger than the simulation volume, which considers only a half-sarcomere of one myofibril. Counter-balancing these concerns, we note that (a) the basic structure of both frog twitch fibers and mouse fast-twitch fibers is a highly repetitive one that is reflected in the sarcomeric and myofibrillar features incorporated into the model, and (b) the measurement and simulation of the Δf_{CaD} signal in frog fibers revealed clear differences when compared with that in mouse fibers. Nevertheless, it would clearly be advantageous to have an experimental method that more directly assessed the properties of the inferred Ca²⁺ release waveforms in the two fiber types. It does not appear that a straightforward use of spatially resolved imaging techniques to measure a Ca²⁺-indicator signal in response to AP stimulation (e.g., as used by Escobar et al., 1994; Monck et al., 1994; Hollingworth et al., 2000; and Zoghbi et al., 2000) would be useful in this regard. These measurements, as well as those in this study, monitor a signal that is directly related to Δ [Ca²⁺] rather than the Ca²⁺ release waveform per se (whose time course is quite different from that of Δ [Ca²⁺]). Indicator-dye measurements that more directly monitor the Ca²⁺ release waveform can be made if a large concentration of an exogenous high-affinity Ca²⁺ buffer is present in the myoplasm (e.g., Baylor and Hollingworth, 1988; Jong et al., 1995; Pape and Carrier, 1998); with this approach, however, any process dependent on CICR, as proposed for activation of the parajunctional Ca²⁺ release channels, would be expected to be suppressed. A pharmacological approach might provide a successful test for the presence of two kinetically distinguishable release components in fibers with both junctional and parajunctional receptors; for example, if a releasechannel inhibitor were available that was selective for RyR β over RyR α and did not affect other processes in the E-C coupling sequence. Unfortunately, we are not aware of the existence of such an inhibitor.

Finally, it should be pointed out that factors other than activation of parajunctional RyRs might contribute to the difference in the measured properties of the Δf_{CaD} signal in frog versus mouse fibers. For example, we cannot rule out the possibility that some difference in the AP or in the functioning of the DHPRs, including the amplitude and time course of muscle charge movement elicited by the AP, occurs in the two fiber types that might contribute to, or perhaps entirely account for, the difference in the Δf_{CaD} signals.

Inactivation of Ca2+ release

If CICR is the mechanism of activation of the parajunctional RyRs and/or the junctional RyRs that are not located directly opposite DHPR tetrads, the potential for a regenerative release of SR Ca²⁺ appears to exist in all skeletal fiber types. In this circumstance, it would be important to have some control capable of inhibiting Ca²⁺ release. The process of Ca²⁺ inactivation of Ca²⁺ release (Baylor et al., 1983; Schneider and Simon, 1988; Baylor and Hollingworth, 1988; Jong et al., 1995) appears capable of supplying this control. In frog cut fibers activated by a step depolarization from -90 mV to a positive potential, Ca²⁺ inactivation of Ca²⁺ release appears to rapidly inhibit >90% of the fiber's Ca²⁺ release capability (Jong et al., 1995). Our experiments on frog intact fibers stimulated by a high-frequency train of APs (Fig. 11 and associated text) are generally consistent with these results and with those of Pape et al. (1993) on cut fibers stimulated by multiple APs. We estimate that, with a 100-Hz stimulus of a frog intact fiber at 16°C, the amount of Ca²⁺ released with the second AP in the train is 20–30% of that of the first release, and, by the 10th AP, the amount is \sim 10% of the first release (Fig. 11). It is likely that this strong suppression of release is due mainly to the process of Ca²⁺ inactivation (Pape et al., 1993; Jong et al., 1995). A rapid onset of Ca²⁺ inactivation of the release system, perhaps in combination with a resting inhibition of parajunctional RyRs due to a myoplasmic free Mg2+ concentration near 1 mM, may be the reason that the slower second component of the release waveform represents only $\sim 20\%$ of the total release (one AP; Figs. 7 and 8), whereas the parajunctional RyRs, whose secondary activation may underlie the slower component of release, are found in numbers approximately equal to that of the junctional RvRs.

Ca²⁺ inactivation of Ca²⁺ release also appears to be of major importance in the control of Ca²⁺ release in fibers that contain only junctional RyRs and have a single RyR isoform, including mammalian fast-twitch fibers (Hollingworth et al., 1996; Baylor and Hollingworth, 2007), mammalian slow-twitch fibers (Baylor and Hollingworth, 2003; Hollingworth et al., 2012), and toadfish superfast fibers (Harwood et al., 2011). When these fibers are stimulated by a train of five APs at 67-83 Hz, the amount of release with the second and subsequent APs is estimated to be 26–15% of the first release in fast-twitch fibers, 30–13% in slow-twitch fibers, and 35–30% in superfast fibers (16°C). Overall, this mechanism (a) prevents [Ca²⁺] from rising to higher levels than is needed to activate the myofilaments, thereby reducing the expenditure of ATP for the resequestration of Ca²⁺; (b) helps avoid unnecessary delays in relaxation; and (c) limits the entry of potentially toxic amounts of Ca²⁺ into the mitochondria.

Possible competition between Mg²⁺ and Ca²⁺ for troponin As mentioned in the Introduction, several reports in the literature suggest that Mg²⁺, at physiological levels, competes with Ca²⁺ for occupancy of the troponin regulatory sites. To our knowledge this possibility has not yet been considered in analyses of Δ [Ca²⁺] measurements in muscle cells. Interestingly, results with our multicompartment modeling (Figs. 8, 10, and 11) are not strongly affected under the hypothesis that Mg²⁺ binds to the troponin regulatory sites with a moderate affinity (dissociation constant = 2 mM; myoplasmic free $[Mg^{2+}] = 1 \text{ mM}$). In comparison with the noncompetitive troponin model, the time course of Ca²⁺ release in frog fibers estimated in these simulations is prolonged slightly due to a modest increase in the amount of the second release component (fractional amount, 0.24 vs. 0.15), the total amount of Ca²⁺ release is reduced by \sim 5%, the peak spatially averaged change in the Ca²⁺ occupancy of the troponin regulatory sites is reduced by \sim 12%, and the peak time of this occupancy is increased from 15 to 20 ms (16°C).

We thank Dr. Clara Franzini-Armstrong for providing the color version of Fig. 1 and Drs. W. K. Chandler and Franzini-Armstrong for discussions.

This work was supported by a grant to S.M. Baylor from the National Institutes of Health (GM 086167).

Richard L. Moss served as editor.

Submitted: 9 January 2013 Accepted: 25 March 2013

REFERENCES

- Allen, T.S., L.D. Yates, and A.M. Gordon. 1992. Ca(2+)-dependence of structural changes in troponin-C in demembranated fibers of rabbit psoas muscle. *Biophys. J.* 61:399–409. http://dx.doi.org/10.1016/S0006-3495(92)81846-5
- Baylor, S.M., and S. Hollingworth. 1988. Fura-2 calcium transients in frog skeletal muscle fibres. *J. Physiol.* 403:151–192.
- Baylor, S.M., and S. Hollingworth. 1998. Model of sarcomeric Ca²⁺ movements, including ATP Ca²⁺ binding and diffusion, during activation of frog skeletal muscle. *J. Gen. Physiol.* 112:297–316. http://dx.doi.org/10.1085/jgp.112.3.297
- Baylor, S.M., and S. Hollingworth. 2003. Sarcoplasmic reticulum calcium release compared in slow-twitch and fast-twitch fibres of mousemuscle. J. Physiol. 551:125–138. http://dx.doi.org/10.1113/ jphysiol.2003.041608
- Baylor, S.M., and S. Hollingworth. 2007. Simulation of Ca²⁺ movements within the sarcomere of fast-twitch mouse fibers stimulated by action potentials. *J. Gen. Physiol.* 130:283–302. http://dx.doi.org/10.1085/jgp.200709827
- Baylor, S.M., and S. Hollingworth. 2011. Calcium indicators and calcium signalling in skeletal muscle fibres during excitation-contraction coupling. *Prog. Biophys. Mol. Biol.* 105:162–179. http://dx.doi.org/10.1016/j.pbiomolbio.2010.06.001
- Baylor, S.M., and S. Hollingworth. 2012. Intracellular calcium movements during excitation-contraction coupling in mammalian slow-twitch and fast-twitch muscle fibers. J. Gen. Physiol. 139:261–272. http://dx.doi.org/10.1085/jgp.201210773
- Baylor, S.M., W.K. Chandler, and M.W. Marshall. 1983. Sarcoplasmic reticulum calcium release in frog skeletal muscle fibres estimated from Arsenazo III calcium transients. *J. Physiol.* 344: 625–666.
- Baylor, S.M., S. Hollingworth, and W.K. Chandler. 2002. Comparison of simulated and measured calcium sparks in intact skeletal muscle fibers of the frog. *J. Gen. Physiol.* 120:349–368. http://dx.doi.org/10.1085/jgp.20028620
- Beam, K.G., and P. Horowicz. 2004. Excitation-contraction coupling in skeletal muscle. *In* Myology. A.G. Engel and C. Franzini-Armstrong, editors. McGraw Hill, New York. 257–280.
- Block, B.A., T. Imagawa, K.P. Campbell, and C. Franzini-Armstrong. 1988. Structural evidence for direct interaction between the molecular components of the transverse tubule/sarcoplasmic reticulum junction in skeletal muscle. *J. Cell Biol.* 107:2587–2600. http://dx.doi.org/10.1083/jcb.107.6.2587
- Brown, I.E., D.H. Kim, and G.E. Loeb. 1998. The effect of sarcomere length on triad location in intact feline caudofeomoralis muscle fibres. *J. Muscle Res. Cell Motil.* 19:473–477. http://dx.doi.org/10.1023/A:1005309107903
- Cannell, M.B., and D.G. Allen. 1984. Model of calcium movements during activation in the sarcomere of frog skeletal muscle. *Biophys. J.* 45:913–925. http://dx.doi.org/10.1016/S0006-3495(84)84238-1
- Cheung, A., J.A. Dantzig, S. Hollingworth, S.M. Baylor, Y.E. Goldman, T.J. Mitchison, and A.F. Straight. 2002. A small-molecule inhibitor of skeletal muscle myosin II. *Nat. Cell Biol.* 4:83–88. http://dx.doi.org/10.1038/ncb734

- Davis, J.P., J.A. Rall, P.J. Reiser, L.B. Smillie, and S.B. Tikunova. 2002. Engineering competitive magnesium binding into the first EF-hand of skeletal troponin C. *J. Biol. Chem.* 277:49716–49726. http://dx.doi.org/10.1074/jbc.M208488200
- Ecob-Prince, M.S., and E. Leberer. 1989. Parvalbumin in mouse muscle in vivo and in vitro. *Differentiation*. 40:10–16. http://dx.doi.org/10.1111/j.1432-0436.1989.tb00808.x
- Eisenberg, B.R. 1983. Quantitative ultrastructure of mammalian skeletal muscle. *In* Handbook of Physiology, Section 10: Skeletal Muscle. L.D. Peachey, R.H. Adrian, and S.R. Geiger, editors. Baltimore: Williams and Wilkins. 73–112.
- Escobar, A.L., J.R. Monck, J.M. Fernandez, and J.L. Vergara. 1994. Localization of the site of Ca2+ release at the level of a single sarcomere in skeletal muscle fibres. *Nature*. 367:739–741. http://dx.doi.org/10.1038/367739a0
- Felder, E., and C. Franzini-Armstrong. 2002. Type 3 ryanodine receptors of skeletal muscle are segregated in a parajunctional position. *Proc. Natl. Acad. Sci. USA*. 99:1695–1700. http://dx.doi.org/10.1073/pnas.032657599
- Fink, R.H.A., D.G. Stephenson, and D.A. Williams. 1986. Calcium and strontium activation of single skinned muscle fibres of normal and dystrophic mice. *J. Physiol.* 373:513–525.
- Franzini-Armstrong, C. 1975. Membrane particles and transmission at the triad. *Fed. Proc.* 34:1382–1389.
- Franzini-Armstrong, C. 1984. Freeze-fracture of frog slow tonic fibers. Structure of surface and internal membranes. *Tissue Cell*. 16:647–664. http://dx.doi.org/10.1016/0040-8166(84)90038-7
- Franzini-Armstrong, C., and J.W. Kish. 1995. Alternate disposition of tetrads in peripheral couplings of skeletal muscle. *J. Muscle Res. Cell Motil.* 16:319–324. http://dx.doi.org/10.1007/BF00121140
- Franzini-Armstrong, C., and G. Nunzi. 1983. Junctional feet and particles in the triads of a fast-twitch muscle fibre. *J. Muscle Res. Cell Motil.* 4:233–252. http://dx.doi.org/10.1007/BF00712033
- Godt, R.E., and B.D. Lindley. 1982. Influence of temperature upon contractile activation and isometric force production in mechanically skinned muscle fibers of the frog. J. Gen. Physiol. 80:279–297. http://dx.doi.org/10.1085/jgp.80.2.279
- Godt, R.E., and D.W. Maughan. 1988. On the composition of the cytosol of relaxed skeletal muscle of the frog. Am. J. Physiol. 254:C591–C604.
- Gómez, J., P. Neco, M. DiFranco, and J.L. Vergara. 2006. Calcium release domains in mammalian skeletal muscle studied with twophoton imaging and spot detection techniques. *J. Gen. Physiol.* 127:623–637. http://dx.doi.org/10.1085/jgp.200509475
- González, A., W.G. Kirsch, N. Shirokova, G. Pizarro, M.D. Stern, and E. Ríos. 2000. The spark and its ember: separately gated local components of Ca²⁺ release in skeletal muscle. *J. Gen. Physiol.* 115:139–158. http://dx.doi.org/10.1085/jgp.115.2.139
- Harwood, C.L., I.S. Young, B.A. Tikunov, S. Hollingworth, S.M. Baylor, and L.C. Rome. 2011. Paying the piper: the cost of Ca²⁺ pumping during the mating call of toadfish. *J. Physiol.* 589:5467–5484. http://dx.doi.org/10.1113/jphysiol.2011.211979
- Heizmann, C.W., M.W. Berchtold, and A.M. Rowlerson. 1982. Correlation of parvalbumin concentration with relaxation speed in mammalian muscles. *Proc. Natl. Acad. Sci. USA*. 79:7243–7247. http://dx.doi.org/10.1073/pnas.79.23.7243
- Hirota, A., W.K. Chandler, P.L. Southwick, and A.S. Waggoner. 1989. Calcium signals recorded from two new purpurate indicators inside frog cut twitch fibers. J. Gen. Physiol. 94:597–631. http://dx.doi.org/10.1085/jgp.94.4.597
- Hollingworth, S., M. Zhao, and S.M. Baylor. 1996. The amplitude and time course of the myoplasmic free [Ca²⁺] transient in fast-twitch fibers of mouse muscle. *J. Gen. Physiol.* 108:455–469. http://dx.doi.org/10.1085/jgp.108.5.455

- Hollingworth, S., C. Soeller, S.M. Baylor, and M.B. Cannell. 2000. Sarcomeric Ca2+ gradients during activation of frog skeletal muscle fibres imaged with confocal and two-photon microscopy. J. Physiol. 526:551–560. http://dx.doi.org/10.1111/j.1469-7793 .2000.t01-1-00551.x
- Hollingworth, S., W.K. Chandler, and S.M. Baylor. 2006. Effects of tetracaine on voltage-activated calcium sparks in frog intact skeletal muscle fibers. J. Gen. Physiol. 127:291–307. http://dx.doi.org/10.1085/jgp.200509477
- Hollingworth, S., M.M. Kim, and S.M. Baylor. 2012. Measurement and simulation of myoplasmic calcium transients in mouse slowtwitch muscle fibres. *J. Physiol.* 590:575–594. http://dx.doi.org/10 .1113/jphysiol.2011.220780
- Jacquemond, V., L. Csernoch, M.G. Klein, and M.F. Schneider. 1991. Voltage-gated and calcium-gated calcium release during depolarization of skeletal muscle fibers. *Biophys. J.* 60:867–873. http://dx.doi.org/10.1016/S0006-3495(91)82120-8
- Johnson, J.D., D.E. Robinson, S.P. Robertson, A. Schwartz, and J.D. Potter. 1981. Ca²⁺ exchange with troponin and the regulation of muscle contraction. *In* Regulation of Muscle Contraction: Excitation-Contraction Coupling. A.D. Grinnell and M.A.B. Brazier. New York: Academic Press. 241–259.
- Jong, D.-S., P.C. Pape, S.M. Baylor, and W.K. Chandler. 1995. Calcium inactivation of calcium release in frog cut muscle fibers that contain millimolar EGTA or Fura-2. J. Gen. Physiol. 106:337– 388. http://dx.doi.org/10.1085/jgp.106.2.337
- Klein, M.G., H. Cheng, L.F. Santana, Y.-H. Jiang, W.J. Lederer, and M.F. Schneider. 1996. Two mechanisms of quantized calcium release in skeletal muscle. *Nature*. 379:455–458. http://dx.doi.org/10.1038/379455a0
- Konishi, M., S. Hollingworth, A.B. Harkins, and S.M. Baylor. 1991. Myoplasmic calcium transients in intact frog skeletal muscle fibers monitored with the fluorescent indicator furaptra. *J. Gen. Physiol.* 97:271–301. http://dx.doi.org/10.1085/jgp.97.2.271
- Kushmerick, M.J., T.S. Moerland, and R.W. Wiseman. 1992. Mammalian skeletal muscle fibers distinguished by contents of phosphocreatine, ATP, and P_{i.} Proc. Natl. Acad. Sci. USA. 89:7521– 7525. http://dx.doi.org/10.1073/pnas.89.16.7521
- Lai, F.A., Q.-Y. Liu, L. Xu, A. el-Hashem, N.R. Kramarcy, R. Sealock, and G. Meissner. 1992. Amphibian ryanodine receptor isoforms are related to those of mammalian skeletal or cardiac muscle. *Am. J. Physiol.* 263:C365–C372.
- Leberer, E., and D. Pette. 1986. Immunochemical quantification of sarcoplasmic reticulum Ca-ATPase, of calsequestrin and of parvalbumin in rabbit skeletal muscles of defined fiber composition. *Eur. J. Biochem.* 156:489–496. http://dx.doi.org/10.1111/j.1432-1033.1986.tb09607.x
- Marx, S.O., K. Ondrias, and A.R. Marks. 1998. Coupled gating between individual skeletal muscle Ca²⁺ release channels (ryanodine receptors). *Science*. 281:818–821. http://dx.doi.org/10.1126/science.281.5378.818
- Melzer, W., E. Rios, and M.F. Schneider. 1987. A general procedure for determining the rate of calcium release from the sarcoplasmic reticulum in skeletal muscle fibers. *Biophys. J.* 51:849–863. http://dx.doi.org/10.1016/S0006-3495(87)83413-6
- Monck, J.R., I.M. Robinson, A.L. Escobar, J.L. Vergara, and J.M. Fernandez. 1994. Pulsed laser imaging of rapid Ca²⁺ gradients in excitable cells. *Biophys. J.* 67:505–514. http://dx.doi.org/10.1016/S0006-3495(94)80554-5
- Morimoto, S. 1991. The effect of Mg2+ on the Ca2+ binding to troponin C in rabbit fast skeletal myofibrils. *Biochim. Biophys. Acta.* 1073:336–340. http://dx.doi.org/10.1016/0304-4165(91)90140-C
- Murayama, T., and Y. Ogawa. 1992. Purification and characterization of two ryanodine-binding protein isoforms from sarcoplasmic reticulum of bullfrog skeletal muscle. *J. Biochem.* 112:514–522.

- O'Brien, J., G. Meissner, and B.A. Block. 1993. The fastest contracting muscles of nonmammalian vertebrates express only one isoform of the ryanodine receptor. *Biophys. J.* 65:2418–2427. http://dx.doi.org/10.1016/S0006-3495(93)81303-1
- O'Brien, J., H.H. Valdivia, and B.A. Block. 1995. Physiological differences between the α and β ryanodine receptors of fish skeletal muscle. *Biophys. J.* 68:471–482. http://dx.doi.org/10.1016/S0006-3495(95)80208-0
- Olivares, E.B., S.J. Tanksley, J.A. Airey, C.F. Beck, Y. Ouyang, T.J. Deerinck, M.H. Ellisman, and J.L. Sutko. 1991. Nonmammalian vertebrate skeletal muscles express two triad junctional foot protein isoforms. *Biophys. J.* 59:1153–1163. http://dx.doi.org/10.1016/S0006-3495(91)82331-1
- Ottini, L., G. Marziali, A. Conti, A. Charlesworth, and V. Sorrentino. 1996. Alpha and beta isoforms of ryanodine receptor from chicken skeletal muscle are the homologues of mammalian RyR1 and RyR3. *Biochem. J.* 315:207–216.
- Oyamada, H., T. Murayama, T. Takagi, M. Iino, N. Iwabe, T. Miyata, Y. Ogawa, and M. Endo. 1994. Primary structure and distribution of ryanodine-binding protein isoforms of the bullfrog skeletal muscle. J. Biol. Chem. 269:17206–17214.
- Paolini, C., F. Protasi, and C. Franzini-Armstrong. 2004. The relative position of RyR feet and DHPR tetrads in skeletal muscle. *J. Mol. Biol.* 342:145–153. http://dx.doi.org/10.1016/j.jmb.2004.07.035
- Pape, P.C., and N. Carrier. 1998. Effect of sarcoplasmic reticulum (SR) calcium content on SR calcium release elicited by small voltage-clamp depolarizations in frog cut skeletal muscle fibers equilibrated with 20 mM EGTA. *J. Gen. Physiol.* 112:161–179. http://dx.doi.org/10.1085/jgp.112.2.161
- Pape, P.C., D.-S. Jong, W.K. Chandler, and S.M. Baylor. 1993. Effect of fura-2 on action potential-stimulated calcium release in cut twitch fibers from frog muscle. J. Gen. Physiol. 102:295–332. http:// dx.doi.org/10.1085/jgp.102.2.295
- Pape, P.C., K. Fénelon, and N. Carrier. 2002. Extra activation component of calcium release in frog muscle fibres. J. Physiol. 542:867–886. http://dx.doi.org/10.1113/jphysiol.2002.017095
- Pizarro, G., L. Csernoch, I. Uribe, and E. Ríos. 1992. Differential effects of tetracaine on two kinetic components of calcium release in frog skeletal muscle fibres. *J. Physiol.* 457:525–538.
- Potter, J.D., and J. Gergely. 1975. The calcium and magnesium binding sites on troponin and their role in the regulation of myofibrillar adenosine triphosphatase. *J. Biol. Chem.* 250:4628–4633.
- Raju, B., E. Murphy, L.A. Levy, R.D. Hall, and R.E. London. 1989. A fluorescent indicator for measuring cytosolic free magnesium. Am. J. Physiol. 256:C540–C548.
- Ríos, E., and G. Brum. 1987. Involvement of dihydropyridine receptors in excitation-contraction coupling in skeletal muscle. Nature. 325:717–720. http://dx.doi.org/10.1038/325717a0
- Ríos, E., and G. Pizarro. 1988. Voltage sensors and calcium channels of excitation-contraction coupling. *Physiology*. 3:223–227.
- Robertson, S.P., J.D. Johnson, and J.D. Potter. 1981. The time-course of Ca2+ exchange with calmodulin, troponin, parvalbumin, and myosin in response to transient increases in Ca2+. *Biophys. J.* 34:559–569. http://dx.doi.org/10.1016/S0006-3495(81)84868-0
- Schneider, M.F., and W.K. Chandler. 1973. Voltage dependent charge movement of skeletal muscle: a possible step in excitation-contraction coupling. *Nature*. 242:244–246. http://dx.doi.org/10.1038/242244a0
- Schneider, M.F., and B.J. Simon. 1988. Inactivation of calcium release from the sarcoplasmic reticulum in frog skeletal muscle. *J. Physiol.* 405:727–745.
- Shirokova, N., J. García, G. Pizarro, and E. Ríos. 1996. Ca²⁺ release from the sarcoplasmic reticulum compared in amphibian and mammalian skeletal muscle. *J. Gen. Physiol.* 107:1–18. http://dx.doi.org/10.1085/jgp.107.1.1

- Smith, D.S. 1966. The organization and function of the sarcoplasmic reticulum and T-system of muscle cells. *Prog. Biophys. Mol. Biol.* 16:107–142. http://dx.doi.org/10.1016/0079-6107(66)90004-6
- Sorrentino, V. 2003. Ryanodine receptor type 3: why another ryanodine receptor isoform? *Front. Biosci.* 8:d176–d182. http://dx.doi.org/10.2741/855
- Stern, M.D., G. Pizarro, and E. Ríos. 1997. Local control model of excitation-contraction coupling in skeletal muscle. *J. Gen. Physiol.* 110:415–440. http://dx.doi.org/10.1085/jgp.110.4.415
- Sutko, J.L., and J.A. Airey. 1996. Ryanodine receptor Ca²⁺ release channels: does diversity in form equal diversity in function? *Physiol. Rev.* 76:1027–1071.
- Tanabe, T., K.G. Beam, J.A. Powell, and S. Numa. 1988. Restoration of excitation-contraction coupling and slow calcium current

- in dysgenic muscle by dihydropyridine receptor complementary DNA. Nature. 336:134-139. http://dx.doi.org/10.1038/336134a0
- Tsugorka, A., E. Ríos, and L.A. Blatter. 1995. Imaging elementary events of calcium release in skeletal muscle cells. *Science*. 269:1723–1726. http://dx.doi.org/10.1126/science.7569901
- Zhao, M., S. Hollingworth, and S.M. Baylor. 1996. Properties of tri- and tetracarboxylate Ca²⁺ indicators in frog skeletal muscle fibers. *Biophys. J.* 70:896–916. http://dx.doi.org/10.1016/S0006-3495(96)79633-9
- Zoghbi, M.E., P. Bolaños, C. Villalba-Galea, A. Marcano, E. Hernández, M. Fill, and A.L. Escobar. 2000. Spatial Ca(2+) distribution in contracting skeletal and cardiac muscle cells. *Biophys. J.* 78:164–173. http://dx.doi.org/10.1016/S0006-3495(00)76582-9